AD NUMBER
ADC003594
CLASSIFICATION CHANGES
TO: **UNCLASSIFIED**
FROM: **CONFIDENTIAL**
LIMITATION CHANGES
TO: **Approved for public release; distribution is unlimited.**
FROM: **Distribution authorized to U.S. Gov't. agencies only; Test and Evaluation; 01 JUL 1975. Other requests shall be referred to Office of Naval Research, One Liberty Center, 875 North Randolph Street, Arlington, VA 22203-1995.**
AUTHORITY
ONR memo dtd 18 Jul 2016; ONR memo dtd 18 Jul 2016

AD-C003594

SECURITY REMARKING REQUIREMENTS

DOD 5200.1-R, DEC 78

REVIEW ON 28 SEP 95

8,051

CONFIDENTIAL

Copy 31 of 60 copies

UNIVERSITY OF MIAMI

ROSENSTIEL SCHOOL OF MARINE AND ATMOSPHERIC SCIENCES

Miami, Fla

2

TECHNICAL REPORT

September 1975

ACOUSTIC COMMUNICATION STUDIES (U)
by
Christopher V. Kimball
to
ADVANCED RESEARCH PROJECTS AGENCY
OFFICE OF NAVAL RESEARCH

CONTRACT N00014-73-C-0434

UM-RSMAS 75034

Since 1 July 1974 the research program described within has been continued at the University of Miami under contract N00014-75-C-0593 by the Office of Naval Research, Code 222.

Arlington, Va. 22217

NATIONAL SECURITY INFORMATION
Unauthorized Disclosure
Subject to
Criminal Sanctions

Distribution limited to U.S. Government Agencies only; Test and Evaluation. 1 July 1975. Other requests for this document should be referred to the Office of Naval Research (Code 222).

CONFIDENTIAL

MIAMI, FLORIDA 33149

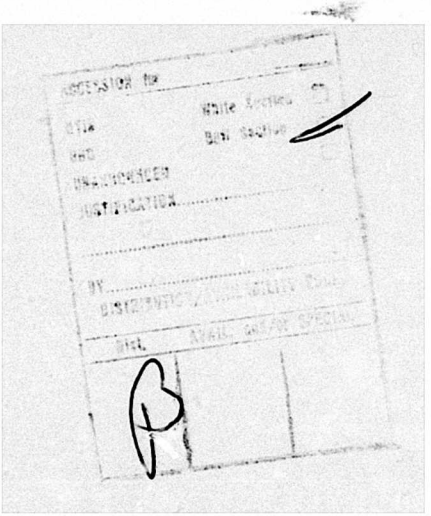
ACCESSION for
NTIS
DDC
UNANNOUNCED
JUSTIFICATION
BY
DISTRIBUTION/AVAILABILITY CODES
DIST. AVAIL. and/or SPECIAL

CONFIDENTIAL

Copy ~~37~~ of 60 copies

UNIVERSITY OF MIAMI

ROSENSTIEL SCHOOL OF MARINE AND ATMOSPHERIC SCIENCES

(12) 38 p.

(9) TECHNICAL REPORT, Jul 71 - Jun 74,

September 1975

(6) ACOUSTIC COMMUNICATION STUDIES (U) (8)

by

(10) Christopher V. Kimball

to

ADVANCED RESEARCH PROJECTS AGENCY
OFFICE OF NAVAL RESEARCH

CONTRACT (11) N00014-73-C-0434 (15)

(14) UM-RSMAS-75034

Since 1 July 1974 the research program described within has been continued at the University of Miami under contract N00014-75-C-0593 by the Office of Naval Research, Code 222.

NATIONAL SECURITY INFORMATION
Unauthorized Disclosure
Subject to
Criminal Sanctions

Distribution limited to U.S. Government Agencies only; Test and Evaluation. 1 July 1975. Other requests for this document should be referred to the Office of Naval Research (Code 222).

CONFIDENTIAL

MIAMI, FLORIDA 33149

405 515

Acoustic Communication Studies (U)

CHRISTOPHER V. KIMBALL

Palisades Geophysical Institute, Miami, Fla.

(Received Aug. 29, 1974)

(C) An experimental study of coherent, matched filter techniques for submarine-to-submarine communication was conducted. Coherent, matched filter techniques offer three advantages over existing systems. First, coherent integration allows useful system operation at signal-to-noise ratios significantly below 0 db. Incoherent systems experience a threshold at a 0-db signal-to-noise ratio, which causes system performance to deteriorate rapidly. Second, filtering of the received information symbol with a filter matched to the received symbol waveform reduces the effects of both noise and multipath. Finally, these techniques are compatible with a wideband, randomized transmission format, which reduces the detectability of the signal by unintended receivers. The research program was conducted in two stages. The first stage evaluated communication system performance over 7- and 42-nmi fixed-site ranges. Over 4,000 hours of experimental data were obtained and analyzed to ensure the statistical significance of the measurements. Results from these data showed that reliable communication could be obtained with signal-to-noise ratios below 0 db. A typical experimental system (M6B) transmitted 0.625 bit/sec in a 100-hz band centered on 420 hz. Over a 42-nmi path, this system yielded a bit error probability of 0.01 at an input signal-to-noise ratio of −9 db. Such performance is within 6 db of that obtainable with the optimum receiver operating through a linear time invariant channel with added white Gaussian noise. To determine the applicability of the fixed-site results to the submarine-to-submarine communication problem, the second stage of the program investigated the space–time stability of the acoustic medium with a towed source. An experiment was conducted in the deep ocean off Eleuthera, B.I. at ranges from 0 to 400 nmi. This experiment indicated only a 10 percent decorrelation in the channel from one 30-sec interval to the next. Consequently, the coherent, matched filter techniques evaluated over the fixed-site ranges are applicable to practical problems involving moving platforms. Based on the results of the experimental program, development of a practical submarine-to-submarine communication system using coherent matched filter techniques is proposed. A particular implementation (M7) incorporating a randomized, burst-type transmission for detection resistance is suggested as a basis for future work.

I. INTRODUCTION

(C) Underwater acoustic communication systems based on coherent, matched-filter techniques have been studied experimentally. Although the specific goal of the research was tactical submarine-to-submarine communication systems, the results are applicable to other situations. This paper describes extensive fixed-site communication experiments and an important transmission measurement that encourage the immediate consideration of these techniques for submarine communication systems.

(C) Coherent, matched-filter techniques offer three distinct advantages for submarine communication systems. First, coherent integration allows satisfactory operation at low signal-to-noise ratios, without the threshold effect that is common to incoherent systems. Second, matched-filter operation reduces the effects of both noise and multipath under varying propagation conditions. And finally, these techniques are compatible with a randomized transmission format that reduces the detectability of the communication signal.

(C) The processing techniques employed in the research are based on well-established theory. The acoustic medium is assumed to approximate a linear, time-invariant channel with added white Gaussian noise. For such a channel, the optimum receiver is composed of a filter matched to the *received* signal, followed by a threshold device. The matched filter can also be shown to reduce intersymbol interference caused by multipath. One of

List of Symbols

$a(i)$	AM sequence coefficient.
$a_P(k, i)$	probe component of kth frame.
$a_I(k, i)$	information component of kth frame.
$a_P(i)$	integrated probe component.
$b(i)$	biphase sequence coefficient.
c	average speed of sound.
$\hat{c}$	estimated average speed of sound.
$d(k, i)$	decision on the ith symbol of the kth frame.
$d'(k, i)$	preliminary decision on the ith symbol of the kth frame.
D	output signal-to-noise ratio.
$e(i)$	ith information bit.
E_P	error count on probe component.
E_I	error count on information component.
E	cumulative error count.
$E\{x\}$	expected value of x.
f_0	carrier frequency.
$\hat{f}_0$	Doppler-shifted carrier frequency.
f_{clk}	receiver clock frequency.
f_{rec}	receiver center frequency.
$g(l)$	transmitted symbol waveform.
$g(k, l)$	transmitted waveform for the kth symbol.
$h(l)$	received symbol waveform.
$h(k, l)$	received waveform for the kth symbol.
K_{cp}	A/D sample compression factor.
K_{fm}	number of sequence periods per frame.
K_{fs}	number of information symbols per frame.
K_{mi}	number of probe frames per measurement interval.
K_{sm}	number of digits per symbol.
K_{sq}	number of digits per sequence period.
$l'(k, j)$	matched filter output for the jth digit of the kth frame.
$l(k, j)$	matched filter output for the jth symbol of the kth frame.
$m(l)$	transmitted waveform.
$m_P(l)$	probe component of transmitted waveform.
$m_I(k, l)$	information component of transmitted waveform.
$n_t(l)$	noise component waveform.
$n(i)$	noise waveform sample.
$\hat{n}(i)$	noise average from probe component.
$n(i, k)$	noise component of matched filter output.
N_{dg}	degree of linear maximal sequence.
N_{fr}	number of symbols per frame.
N_{fm}	number of digits per frame.
n_{mult}	number of multiplications per frame.
N_{sq}	number of samples per sequence period.
NP, NP(k)	noise power in the kth measurement interval.
$p(l)$	received digit waveform.
$\hat{p}(l)$	calculated received digit waveform.
$\hat{p}(k, i)$	sample of calculated digit waveform.
PE	bit error probability.
$q(i)$	symbol composition coefficient for the ith digit.
$q(i, j)$	symbol composition coefficient for the ith digit of the jth symbol.
r'	offset between signal and FFT spectral lines.
r	integer offset between signal and FFT spectral lines.
r^*	value of r which maximizes SNR_{out}.
$R_{xy}(\tau)$	cross correlation between $x(t)$ and $y(t)$.
$\mathcal{R}_{mult}$	multiplication rate.
$s_t(l)$	signal component waveform.
$s(i)$, $s(k, i)$	signal component waveform sample in kth interval.
$S(k, i)$	discrete Fourier transform of $s(k, i)$.
SP, SP(k)	signal power in the kth measurement interval.
SNR_{in}	input signal-to-noise ratio.
SNR_{out}	output signal-to-noise ratio on $a_P(i)$ vector.
T	digit duration.
T_{af}	duration of probe frame plus information frame.
T_{fm}	frame duration.
T_{mi}	duration of measurement interval.
T_{sg}	duration of segment of input.
T'_{sg}	Doppler-distorted segment duration.
T_{sm}	symbol duration.
T_{sq}	sequence-period duration.
$u(t)$	transmitted digit waveform.
$U(t)$	unit step function.
v	source Doppler velocity.
v^*	maximum expected source Doppler velocity.
W	system bandwidth.
W_{lp}	low pass system bandwidth.
$x_t(l)$	received waveform.
$x'(i)$	sample of received waveform.
$x(i)$, $x(k,i)$	compressed sample of received waveform.
$x_P(l)$	probe component of received waveform.
$x_P^\infty(l)$	received waveform from infinitely long probe.
$x_P^E(l)$	periodically extended probe component of received waveform.
$x_I(l)$	information component of received waveform.
$z(k, i)$	complex, compressed sample of received waveform.
$Z(k, i)$	discrete Fourier transform of $z(k, i)$.
σ_n^2	noise variance.
χ^2	chi-squared probability distribution.
$\Phi(u)$	normal cumulative probability distribution.
$\gamma(k, i)$	decision threshold on ith symbol of kth frame.
η	performance differential.
$\delta_{FFT}(i)$	frequency offset between signal and FFT lines.
$\rho(\tau)$	normalized cross correlation function.
$\rho_i^*(i)$	ith correlation coefficient from September 1973 experiment.
$\rho(k, j)$	sample of normalized cross correlation function in kth measurement interval.
$\rho_2^*(k)$	correlation coefficient in kth measurement interval from January 1974 experiment.
$[x]$	greatest integer in x.

the most interesting results of the research is the agreement obtained between the experimental data and the predictions of this theory.

(C) Because the physical channel is distinctly time-varying, the received symbol waveform must be continually measured to maintain the required match between the filter and the symbol waveform. This measurement is made possible by including a known probe component in the transmission in addition to the unknown information component. Thus, the communication systems described here perform dual roles—channel measurement and information transmission.

(U) The experimental program has two closely related stages. The first stage conducted communication experiments between fixed sites to obtain a statistically significant quantity of performance data. Table 1 depicts the history of the fixed-site communications experiment. Only the results of the recent experiments, M5 and M6, are presented here. Previous experiments obtained similar results, but they were based on very few data.[2,3] Sections II, III, and IV of this article detail the operation and performance of the M5 and M6 experiments.

(U) The second stage of the experimental program was to determine the applicability of the fixed-site results to the submarine communication problem. For such an application to be possible, the acoustic medium must be stable in space as well as time. That is, the probe measurement of the channel must remain valid under spatial displacement of the submarine platform. Consequently, a careful measurement of the spatial stability was made, as described in Section V.

(C) The union of the results from the fixed-site communication experiments and the spatial-stability measurements solidly indicates the feasibility of coherent, matched-filter techniques for submarine communication systems. This conclusion and others are presented in Section VI. An application of these techniques in conjunction with a randomized transmission format is also given.

II. TRANSMISSION FORMAT

(C) Because of the dual nature of the transmission and the implementation of the receiver processing,

TABLE 1. *Summary of fixed-site communication experiments. (Table unclassified.)*

Experiment	Year	Distance (nm)	Duration (hr)
M1	1968	7	24
M2	1969	7	24
M3	1969	7	24
M4	1970	42	4
M5A	1972	7	2214
M5B	1972	7	1500
M6A	1973	42	168
M6B	1973	42	984
M6C	1973	42	140

the signals transmitted by the communication systems have a complicated format. One part of the signal, the probe component, allows measurement of the channel; the other, the information component, contains the information. Subsequent parts of this section describe these components in detail and explain the choice of transmission format. Section III on receiver processing completes the explanation. The probe and information components are transmitted interleaved in time (time multiplexed) as described in Section IID.

A. BASIC SIGNAL ELEMENT, THE DIGIT

(U) Both components of the transmission are composed of a succession of biphase modulated elements, called digits. The simplest example of a digit waveform is a rectangular carrier pulse. The probe and information components consist of modulated digits in a prescribed (or in the case of the information component, almost prescribed) order. In the subsequent discussion, no conflict will arise if the digit waveform is assumed to be a rectangular carrier pulse, although in practice, some amount of bandspreading of the digit is desirable, as suggested below.

(U) For a rectangular carrier pulse, the pulse duration and bandwidth are inversely related; that is, once the duration is specified, the bandwidth is also fixed. This constraint is undesirable in practice, since the choice of digit duration and digit bandwidth is based on different considerations. Typically, the digit duration is

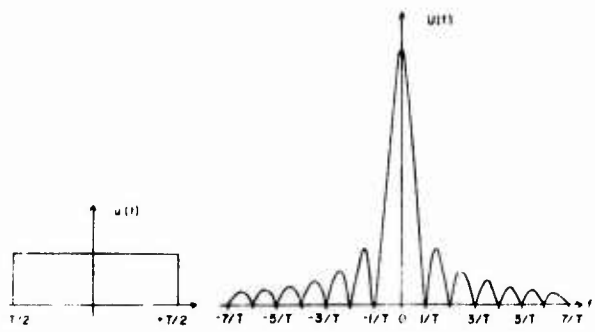

Figure 1a. Digit waveforms: rectangular digit. (Figure unclassified.)

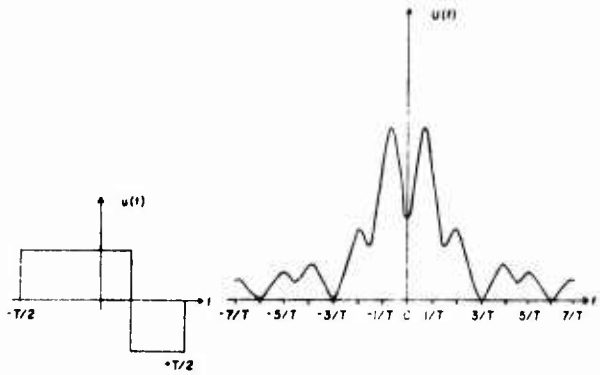

Figure 1b. Digit waveforms: bandspread digit with three subelements. (Figure unclassified.)

selected on the basis of multipath conditions, while the digit bandwidth is based on the transducer bandwidth.

(C) In general, the problem is to increase the digit bandwidth beyond that of a rectangular digit of equal duration. Figure 1 shows the results of bandspreading of the digit waveform by comparison with a rectangular pulse and its spectrum in Fig. 1a. In each part of Fig. 1, $u(t)$ is the digit waveform and $U(f)$ is the digit spectrum. Note that as the number of subelements in the digit waveform is increased, the bandwidth increases proportionately. The digit waveform in Fig. 1b was used in the M1, M2, M3, and M4 experiments, and the waveform in Fig. 1c was used in the M6B and M6C experiments.

B. PROBE COMPONENT

(C) The probe component of the transmission allows the receiver to measure the channel digit

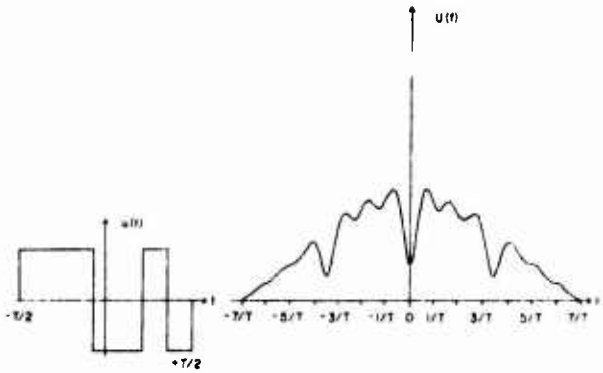

Figure 1c. Digit waveforms: bandspread digit with seven subelements. (Figure unclassified.)

response. Because the information symbols are composed of combinations of digits, a filter matched to the symbols can be formed from the digit response. The probe component must be constant and known to the receiver if this measurement is to be successful. This is in contrast to the information component, described later in Section IIc, which is inherently variable and unknown.

(U) One method of measuring the channel digit response is to transmit a single, isolated digit as the probe component, as shown in Fig. 2a. Vacant time intervals must be included before and after the probe digit to allow for the time smear of the acoustic channel. The disadvantage to this probe structure is that energy is transmitted for only a small fraction of the probe duration. Consequently, the receiver's measurement of the channel is noisy.

(U) A better choice for the probe component is to form it from an integral number of periods of a linear maximal sequence. This allows more energy to be transmitted in the probe, with a corresponding improvement in the measurement of the channel digit response.

(U) Let $u(t)$ be the transmitted digit waveform of duration T. Let $b(i)$, equal to either $+1$ or -1 $[b(i)\epsilon\{\pm 1\}]$, be the values of a K_{sq} long, linear, maximal sequence. The probe component, $m_P(t)$, of the transmission is obtained by modulating successive digits with K_{tm} periods of the sequence:

$$m_P(t) = \sum_{i=0}^{N_{tm}-1} b(i)u(t-iT) \qquad (1)$$

where

$$N_{tm} = K_{sq} \cdot K_{tm} \qquad (2)$$

The transmitted probe component will be time-limited to a duration $T_{fm}=N_{fm}\cdot T$, because of the limited duration of the individual digits. A probe component of this form is shown in Fig. 2b for $K_{fm}=1$ and $K_{sq}=15$.

(U) Because of the assumed linearity of the acoustic channel, the received probe $r_P(t)$ is a superposition of channel digit responses, $p(t)$.

$$r_P(t)=\sum_{i=0}^{N_{fm}-1} b(i)p(t-iT) \tag{3}$$

In general, time smearing of the channel will make the duration of the received probe longer than T_{fm}.

(U) The primary objective of the probe component is to allow measurement of $p(t)$; and consequently $r_P(t)$, as indicated in Eq. (3), must be processed further to be useful. A simple digital filter can be applied to $r_P(t)$ to obtain a waveform $\hat{p}(t)$, which approximates the channel digit response $p(t)$. To understand the derivation of the approximate channel response $\hat{p}(t)$, consider the following analysis for an infinitely long periodic probe component, $r_P^{\infty}(t)$

$$r_P^{\infty}(t)=\sum_{i=-\infty}^{+\infty} b(i)p(t-iT) \tag{4}$$

Define $\hat{p}^{\infty}(t)$, the calculated channel response, as follows:

$$\hat{p}^{\infty}(t)=\sum_{j=0}^{N_{fm}-1}\frac{b(j)+1}{2}\,r_P(t+jT) \tag{5}$$

Note that, although $r_P^{\infty}(t)$ is of infinite extent, the summation for $\hat{p}^{\infty}(t)$ involves only N_{fm} terms.

(U) If Eq. (4) is inserted into Eq. (5), the following expression is obtained:

$$\hat{p}^{\infty}(t)=\sum_{j=0}^{N_{fm}-1}\sum_{i=-\infty}^{+\infty}\frac{b(j)+1}{2}\,b(i)p[t-(i-j)T] \tag{6}$$

After a change of variables, $k=i-j$, Eq. (6) becomes

$$\hat{p}^{\infty}(t)=\sum_{k=-\infty}^{+\infty} p(t-kT)\sum_{j=0}^{N_{fm}-1}\frac{b(j)+1}{2}\,b(j+k) \tag{7}$$

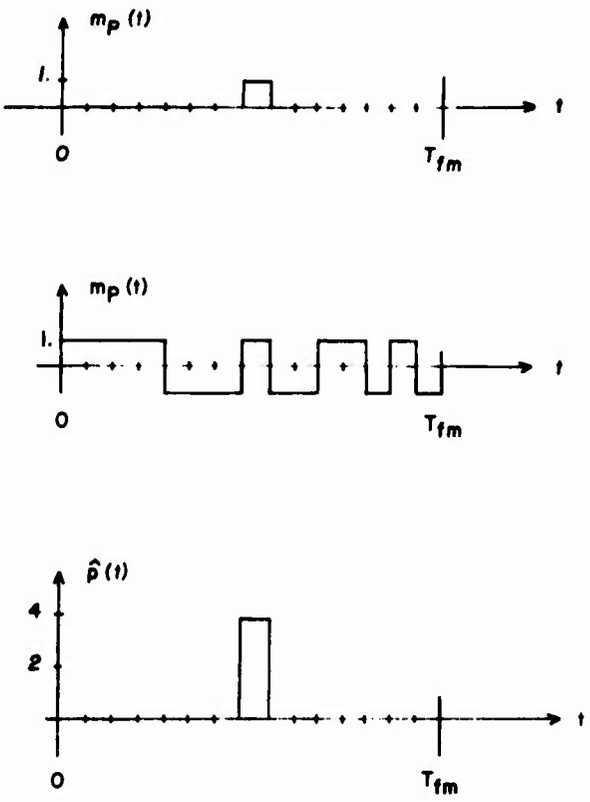

Figure 2. Probe component structures. (Figure and figure caption each classified Confidential.)

Because of the properties of linear maximal sequences, the summation over j is known:

$$\sum_{j=0}^{N_{fm}-1}\frac{b(j)+1}{2}\,b(j+k)=\frac{K_{sq}+1}{2}\cdot K_{fm} \tag{8}$$

for $k=0,\ K_{sq},\ 2K_{sq},\ \ldots$

$$\sum_{j=0}^{N_{fm}-1}\frac{b(j)+1}{2}\,b(j+k)=0 \tag{9}$$

otherwise. With the above results substituted into Eq. (7), the following simplified expression is obtained:

$$\hat{p}^{\infty}(t)=\frac{K_{sq}+1}{2}\,K_{fm}\sum_{i=-\infty}^{+\infty} p(t-K_{sq}\cdot iT) \tag{10}$$

That is, $\hat{p}^{\infty}(t)$ is a periodic (with period $T_{sq}=K_{sq}\cdot T$) replica of $p(t)$ with a processing gain of $K_{fm}\cdot(K_{sq}+1)/2$. Consequently, with an infinitely long probe component, Eq. (5) allows the exact measurement of the channel digit response.

(C) The probe component, $s_P(t)$, for an actual communication system cannot have infinite extent, as does $s_P^{\infty}(t)$. However, a periodic extension, $s_P^{E}(t)$, can be constructed from $s_P(t)$ to yield an approximation to $p(t)$. Assume that most of the energy of $s_P(t)$ is contained in the time interval (t_0, t_0+T_{fm}). Consider the infinite periodic extension, $s_P^{E}(t)$, of $s_P(t)$ in this interval:

$$s_P^{E}(t) = s_P(t); \quad t_0 \le t < t_0 + T_{fm} \tag{11}$$

$$= s_P(t - kT_{fm}); \quad t_0 + kT_{fm} \le t < t_0 + (k+1)T_{fm} \tag{12}$$

If $K_{fm} > 1$ and the time duration of $p(t)$ is small relative to the sequence duration, $T_{sq} = K_{sq} \cdot T$, then

$$s_P^{E}(t) \cong s_P^{\infty}(t) \tag{13}$$

So an approximation to $p(t)$ is calculated as:

$$\hat{p}(t) \quad \sum_{j=0}^{N_{fm}-1} \frac{b(j)+1}{2} s_P^{E}(t); \quad t_0 \le t \le T_{sq} \tag{14}$$

$$\cong \frac{K_{sq}+1}{2} \cdot K_{fm} p(t); \quad t_0 \le t < t_0 + T_{sq} \tag{15}$$

That is, $\hat{p}(t)$ is approximately equal to $p(t)$ multiplied by a constant. This constant gives a significant processing gain against noise.

(C) In the M5 and M6 systems, K_{sq} was selected during the system design stage to be 15, so T_{sq} exceeded the expected smear of $p(t)$ by a factor of at least three. The constant K_{fm} was selected to be four so as to support the approximation indicated by Eq. (13). With these parameter values, the use of the coded probe component yielded a 9-db processing gain over a single digit probe repeated K_{fm} times. No adverse effects due to the approximation were observed.

C. INFORMATION COMPONENT

(C) The information component can be formed in one of three ways: (*1*) biphase modulation of single transmitted digits; (*2*) biphase modulation of groups of digits, where the intragroup structure is constant; or (*3*) variable symbol modulation, in which biphase modulation of groups of digits, where the intragroup structure varies from one symbol to the next, is carried out.

(C) In the subsequent discussion, the difference between a digit—described previously—and a symbol is important. A symbol is a digit or group of digits used to carry a single bit of information. The objective of the receiver is to determine symbol values, not digit values; thus, the difference between the two methods of forming the information component lies in the structure of the symbol waveform.

1. Single Digit Symbols

(U) The simplest construction of the information component assigns a single digit to each symbol. A digit transmitted at 0 phase represents a binary one; a digit transmitted at 180-deg phase represents a binary-minus one. This technique was used in the M1, M2, M3, and M4 systems.

(C) In all of the systems considered, the number of digits in the information component was made equal to the number of digits in the probe component. When the probe component contained K_{fm} repetitions of the K_{sq} digit linear maximal sequence, the information component was composed of K_{fm} repetitions of K_{sq} information-bearing digits. This symmetric structure is arbitrary, and it effectively sets the information and probe component energies equal. In general, the structures of the probe and information components are independent, subject only to the constraint that both be composed of the same digit waveform. Thus, the kth transmitted information component $m_I(k, t)$ is given by

$$m_I(k, t) \quad \sum_{i=0}^{K_{fm}-1} \sum_{j=0}^{K_{sq}-1} e(K_{sq} \cdot k + j)\, a[t - (K_{sq} \cdot i + j)T] \tag{16}$$

where $e(n) \in \{\pm 1\}$ is the nth information bit.

(U) Figure 3a depicts an information component using a single digit per symbol. The diagram shows K_{sq} symbols corresponding to the information stream $-1+1-1+1+1+1$, $-1-1+1-1-1-1$, $-1+1+1+1+1+1$. Only one repetition ($K_{fm} = 1$) is shown for simplicity. In actual practice K_{fm} is taken as being larger than one to increase the energy content of each symbol and to provide limited time diversity.

2. Multiple Digit Symbols

(C) If each information symbol is composed of only one digit, as described above, then potential

tradeoff opportunities for system design are eliminated. For example, the number of digits in the sequence, K_{sq}, and the digit duration, T, must be selected so that the time duration of the received digit, $p(t)$, is less than the sequence period, T_{sq}, in order to properly measure $p(t)$. Because of memory requirements in the receiver, the sequence period, T_{sq}, should be as short as possible. However, the resulting digit duration, T, may be too small to provide adequate symbol energy and to avoid intersymbol interference.

(C) One solution to the above problem is to simply allow more than one digit per symbol, keeping the digit duration, T, and K_{sq} constant. In the M5 and M6 systems, three digits were used for each information symbol, giving a threefold increase in both symbol energy and duration, with no increase in sequence duration, T_{sq}.

(C) The composition of the information symbol is arbitrary, as long as it is composed of linear combinations of digit waveforms. Let $g(t)$ be a symbol that is taken as being composed of K_{sm} digit waveforms,

$$g(t)=\sum_{i=0}^{K_{sm}-1} q(i)u(t-iT) \qquad (17)$$

where $q(i)\epsilon\{\pm 1\}$; $i=0, \ldots, K_{sm}-1$. The choice of digit separations of multiples of T sec and unity magnitudes for the $q(i)$'s is not essential in general, but it was made for ease of generation and processing of the signal. If $p(t)$ is the received digit response, then a filter, $h(t)$, matched to the received symbol is

$$h(t)=\sum_{i=0}^{K_{sm}-1} q(i)p(t-iT) \qquad (18)$$

by the assumed linearity of the channel. Thus, a filter matched to a specified symbol can easily be constructed from the received digit waveform $p(t)$ and the symbol composition given by $q(0), \ldots, q(K_{sm}-1)$.

(U) Figure 3b depicts an information component with $K_{sm}=3$ digits per symbol and with $q_0=1$, $q_1=1$, and $q_2=-1$. The information values shown are $-1+1-1+1+1$. Again, $K_{fm}=1$ for the sake of simplicity.

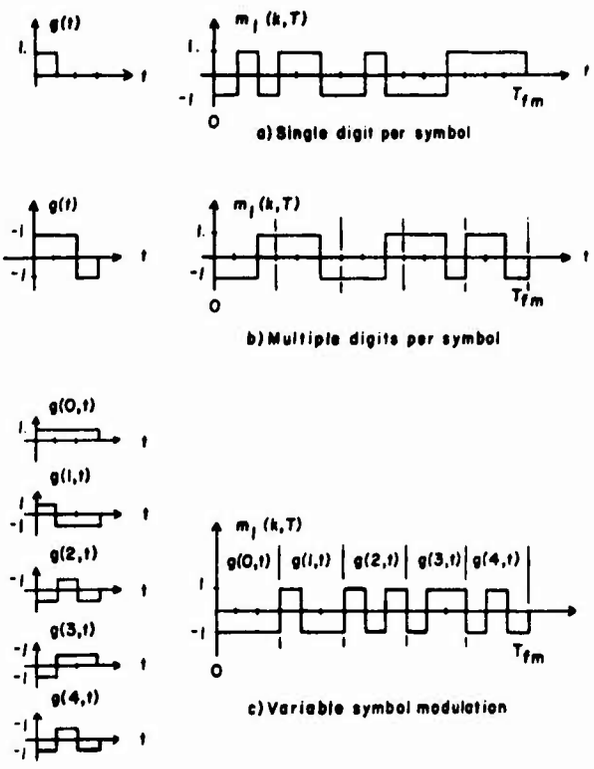

Figure 3. Information component structures. (Figure and figure caption each classified Confidential.)

3. *Variable Symbol Modulation*

(C) If more than one digit is contained in each symbol, as described above, the opportunity to alter the symbol composition from one time interval to the next arises. For example, consider K_{fs} consecutive symbols having K_{sm} digits per symbol. The jth symbol waveform is specified by K_{sm} coefficients, $q(0) \ldots q(K_{sm}-1)$, $q(i)\epsilon\{\pm 1\}$, giving a possibility of $2^{K_{sm}}$ different symbol waveforms. There is no requirement that successive symbols have the same composition, so one could define K_{sf} symbol waveforms $g(j,t)$ $j=0 \ldots K_{sf}-1$, each with different composition,

$$g(j,t)=\sum_{i=0}^{K_{sm}-1} q(j,i)u(t-iT); \quad j=0 \ldots K_{sf}-1 \qquad (19)$$

to be transmitted $T_{sm}=K_{sm}T$ sec apart. Because of the assumed linearity of the channel, a filter matched to each symbol, $h(j,t)$, can easily be

constructed from $p(t)$. The kth transmitted probe component $m_1(k,t)$ is then

$$m_1(k,t)=\sum_{i=0}^{K_{fm}-1}\sum_{j=0}^{K_{fs}-1} e(K_{fs}\cdot k+j) \times g(j, t-j\cdot T_{sm}-iT_{sq}) \quad (20)$$

The technique in which the symbol composition is permitted to vary from one symbol to the next is called variable symbol modulation.

(C) Variable symbol modulation was incorporated into the M5 and M6 communication systems as a means of facilitating the experimental measurement of system performance. In Section VIB, variable symbol modulation is shown to be an important component of a detection-resistant transmission format. In the M5 and M6 systems, the product of K_{sm} and K_{fs} was selected to equal K_{sq}, specifically, $K_{sm}=3$, $K_{fs}=5$. Under these conditions, the probe and information components can be made identical by a proper choice of $q(i,j)$ and the information values $e(i)$.

(C) Let

$$q(j,i)=b(K_{sm}\cdot j+i);$$
$$i=0\ldots K_{sm}-1 \text{ and } j=0\ldots K_{fm}-1 \quad (21)$$

where $b(i)$, $i=0\ldots K_{sq}-1$ are the biphase sequence coefficients described in Section IIB. Then if $e(j)=1$, for all j, the transmitted information component is

$$m_1(k,t)=\sum_{i=0}^{K_{fm}-1}\sum_{j=0}^{K_{fs}-1} e(K_{sf}\cdot k+j)\sum_{n=0}^{K_{sm}-1} q(j,n) \times u[t-(iT_{sg}+jT_{sm}+nT)] \quad (22)$$

$$=\sum_{i=0}^{K_{fm}-1}\sum_{j=0}^{K_{sq}-1} b(j)u[t-(K_{sq}\cdot i+j)T] \quad (23)$$

$$=\sum_{i=0}^{N_{fm}-1} b(j)u(t-jT) \quad (24)$$

which is exactly the same as the probe component given by Eq. (3).

(U) The advantage of the above choice of K_{sm}, K_{fs}, $q(i,j)$, and $e(i)$ is that, since the probe and information components are identical, a periodic transmission is a valid system transmission. In measurement of the communication performance of the M5 and M6 systems, such a periodic waveform was transmitted. This simplified the structure of the transmitter and eliminated the need for synchronization of the receiver during the lengthy evaluation process.

(U) Figure 3c depicts an information component with variable symbol modulation. The information values being transmitted are -1, $+1$, -1, $+1$, $+1$, and $K_{fm}=1$.

D. MULTIPLEXING OF PROBE AND INFORMATION COMPONENTS

(C) The transmission in each of the matched-filter communication systems consists of a multiplex of the probe and information components. In choosing the multiplexing technique, the particular purpose of the probe component must be considered. For example, frequency multiplexing would be inappropriate in the acoustic medium, because the digit response measured in one frequency band would not be valid in another frequency band. Two suitable multiplexing techniques are time multiplexing and phase multiplexing. The M5 and M6 systems used time multiplexing, as described below. Later, in Section VIB, an application of phase multiplexing is presented.

(C) In the M5 and M6 systems, the transmission $m(t)$ was composed of a simple time multiplex of probe and information components:

$$m(t)=\sum_{i=-\infty}^{+\infty} m_P(t-2T_{fm}\cdot i)+m_I[i, t-(2i+1)T_{fm}] \quad (25)$$

where T_{fm} is the probe (and information) component duration and $T_{fm}=K_{fm}\cdot K_{sq}\cdot T$. Thus, the transmission consists of alternating probe and information components, with each successive information component representing different information bits. Figure 4 depicts a typical transmission from the M5 and M6 systems. The information values for the information component shown in expanded form are -1, $+1$, -1, $+1$, -1.

III. RECEIVER PROCESSING

(C) The receiver in the M5 and M6 communication systems performs a dual role. The first part of this dual role is to measure the existing channel digit response from the probe component of the transmission. Several additional measurements are made from the probe in order to eval-

nate system performance. The second part of the receiver's role is to determine the transmitted symbol values. In general, time synchronization is required to direct the probe component of the transmission to the probe processing section of the receiver, etc. This synchronization is discussed in Section IIID, while the following discussion (particularly Sections IIIB and IIIC) assumes that correct synchronization has already been obtained.

A. PRELIMINARY PROCESSING

(U) Signals from the receiver hydrophone are transmitted through linear, fixed-gain amplifiers to the processor, the gains of these amplifiers being selected so that no clipping occurs during normal operation. At the processor site, a fixed analog filter centered on the carrier wave, 420 hz, and with nominal bandwidth of 100 hz removes much of the ambient noise from the signal. The output of the filter is amplified by another fixed-gain amplifier and applied to the digital processor analog-to-digital converter.

(U) The analog converter in the processor handles signals in the ±1-volt range and has either 8 bit (M5) or 9 bit (M6A, M6B, M6C) plus sign resolution, with the equivalent dynamic ranges being 48 and 54 db, respectively. System gains are adjusted so that normal operation occurs at roughly 10 db below the converter limit. Local shipping noise does cause overloads to occur throughout the system, but these overloads are infrequent and are easily recognized.

(U) The sampling of the bandpass input signal is controlled by a high-stability oscillator (at least 1 part in 10^7) set for a sampling rate f_{clk} of four times (1680 hz) the carrier frequency. The samples, $s'(i)$, are digitally processed to obtain complex low-pass samples, $s(i)$, equivalent to the original bandpass waveform.

$$s(i)=\frac{1}{K_{cp}}\sum_{j=0}^{K_{cp}-1}(-1)^j s'(2K_{cp}\cdot i+2j) \quad (i \text{ even}) \tag{26}$$

$$s(i)=\frac{1}{K_{cp}}\sum_{j=0}^{K_{cp}-1}(-1)^j \times s'[2K_{cp}\cdot(i-1)+2j+1] \quad (i \text{ odd}) \tag{27}$$

In the above equations, K_{cp} is the compression factor. The samples $s(i)$ with even indices can be

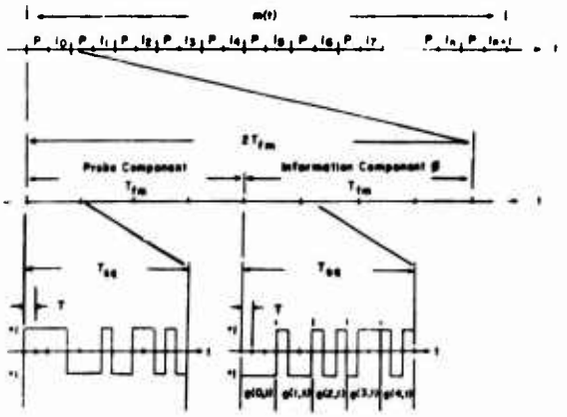

Figure 4. Typical transmission from the M5 and M6 systems. (Figure classified Confidential.)

associated with the real component of the signal, and the odd indices can be associated with the imaginary component. The equivalent low-pass bandwidth W_{lp} of either component is given by

$$W'_{lp}=\frac{f_{clk}}{4K_{cp}} \tag{28}$$

where f_{clk} is the sampling frequency.

(U) Two additional constants will be helpful in working with the compressed samples $s(i)$ of the input waveform. The first is the number of samples per digit, N_{dg}, given by

$$N_{dg}=\frac{f_{clk}\cdot T}{K_{cp}} \tag{29}$$

The second constant is the number of compressed samples per sequence period N_{sq}:

$$N_{sq}=K_{sq}\cdot N_{dg} \tag{30}$$

As will be seen shortly, N_{sq} is an important constant in determining the memory requirements of the receiver.

B. PROBE PROCESSING

(C) The primary objective of the probe processing is to determine the channel digit response, $p(t)$. A secondary, but important, objective of the probe processing is to measure the basic transmission characteristics of the medium to aid in evaluation and understanding of the system performance. All of the communications systems included measurement of the wideband signal power and

noise power, SP and NP, while several specialized measures of the time smear and time stability of the channel are also derived from $p(t)$.

(C) The probe processing operates on the probe component of the transmission. At the input signal-to-noise ratios below 0 db for which the systems were designed, the energy contained in a single probe component is inadequate for obtaining a satisfactory estimate of the channel digit response, $\hat{p}(t)$. Because of this, coherent integration of K_{m1} probe components is performed, with the time interval over which it is performed being called the measurement interval. To reduce the receiver memory requirements, this integration is performed in two steps.

(C) The first step is to integrate over the K_{fm} sequence periods contained in a single probe component to yield a single vector of length N_{sq}. Let $a_P(k, i)$ be the ith element of this vector, derived from the kth probe component. That is,

$$a_P(k, i)=\sum_{j=0}^{K_{fm}-1} x(2\cdot k\cdot N_{sq}\cdot K_{fm}+j\cdot N_{sq}+i)$$
$$0\leq k<K_{m1};\quad 0\leq i<N_{sq} \tag{31}$$

The above equation assumes that the receiver has been synchronized so that $x(0)\ldots x(N_{sq}\cdot K_{fm}-1)$ are samples of a probe component.

(C) The second step in the integration of the K_{m1} probe components is to derive the signal vector $a_P(i)$:

$$a_P(i)=\sum_{k=0}^{K_{m1}-1} a_P(k, i) \tag{32}$$

The signal vector $a_P(i)$ is the coherent integration of $K_{fm}\cdot K_{m1}$ sequence periods and is the starting point in the determination of the channel digit response, $\hat{p}(t)$. At the same time, another vector of N_{sq} points is also calculated.

$$\hat{n}(i)=\sum_{k=0}^{K_{m1}-1}(-1)^k a_P(k, i) \tag{33}$$

The noise vector, $\hat{n}(i)$, eliminates the signal contribution by alternating the sign in its summation, and it is the basis for the noise power measurement.

1. Channel Digit Response Measurements

(U) As mentioned above, the primary objective of the probe processing is to derive the approximate channel digit response $\hat{p}(t)$. Let $\hat{p}(k,i)$ be the sampled data representation of $\hat{p}(t)$ obtained in the kth measurement interval. From a discrete version of the derivation of Section IIB, the following result is obtained:

$$\hat{p}(k, i)=\sum_{j=0}^{K_{sq}-1}\frac{b(j)+1}{2}a_P(i+j\cdot N_{dg});\quad 0\leq i<N_{sq} \tag{34}$$

where the index $i+j\cdot N_{dg}$ is taken *modulo* N_{sq}. The index k on $\hat{p}(k, i)$ is introduced at this point to facilitate subsequent description; it indicates that $\hat{p}(k, i)$ is derived from the kth measurement interval of k_{m1} probe components.

(U) An oscilloscope display of the $\hat{p}(k, i)$ vector is provided, and it is updated during each measurement interval by the processor. Unfortunately, the N_{sq} points in the display are too many to be retained during a long-term experiment; however, two useful measures of the multipath situation are recorded for evaluation of system performance.

(U) The first multipath measure is the autocorrelation of the channel digit response, $\hat{p}(k, i)$, taken at multiples of the digit length, N_{dg}.

$$R_{\hat{p}\hat{p}}(k, iN_{dg})=\sum_{j=0}^{N_{sq}-1}\hat{p}(k, j)$$
$$\times\ \hat{p}(k, j+iN_{dg});\quad i=0\ldots 6 \tag{35}$$

where the index $j+iN_{dg}$ is taken *modulo* N_{sq}. These measurements are indicative of the time smear of the channel, and they are important in measuring the extent of intersymbol interference. For example, if the channel were ideal (broad band) then $\hat{p}(k, j)$ and $\hat{p}(k, j+iN_{dg})$ would have no overlap for $i>0$. Then $R_{\hat{p}\hat{p}}(k, iN_{dg})$ would be zero for $i>0$. Thus, as $R_{\hat{p}\hat{p}}(k, iN_{dg})$ with $i>0$ becomes large relative to $R_{\hat{p}\hat{p}}(k, 0)$, the time smear of the channel increases.

(U) The second multipath measure is the cross correlation between two consecutive measurements of $\hat{p}(k, t)$. Let $\hat{p}(k-1, t)$, $\hat{p}(k, t)$ be two digit response measurements, based on consecutive but nonoverlapping measurement intervals. Then, the normalized cross correlation coefficient, $\rho(k)$, between the two measurements at zero offset is given by

$$\rho(k)=\frac{\sum_{i=0}^{N_{sq}-1}\hat{p}(k-1, i)\hat{p}(k, i)}{\sqrt{R_{\hat{p}\hat{p}}(k-1, 0)R_{\hat{p}\hat{p}}(k, 0)}} \tag{36}$$

The magnitude of $\rho(k)$ is always less than one. If the acoustic channel were truly time invariant (and there were no noise), then $\rho(k)$ would equal one. If the channel was completely unstable so that the two parameters $\hat{p}(k-1, i)$ and $\hat{p}(k, i)$ had nothing in common, then $\rho(k)$ would have a mean value of zero.

2. Measurement of Signal and Noise Powers

(U) The wideband signal and noise powers, SP and NP, are measured to allow evaluation of system performance. Let $s(i)$ be the signal contribution to the ith sample in a single received sequence period, and let $n(i)$ be the noise contribution to the ith sample in a single received sequence period. The noise contributions $n(i)$ are assumed to be normally distributed with zero mean and variance σ_N^2 and are also assumed to be independent. Then, if the channel is stable,

$$a_P(i) = K_{fm} \cdot K_{mf} s(i) + \sum_{j=0}^{K_{fm}K_{mf}-1} n(j \cdot N_{sq} + i) \tag{37}$$

Then $a_P(i)$ will be of mean $K_{fm}K_{mf}s(i)$ and variance $K_{fm} \cdot K_{mf}\sigma_N^2$. The average signal-to-noise ratio (mean-squared to variance ratio) on $a_P(i)$, SNR_{out} is then

$$SNR_{out} = K_{fm}K_{mf} \sum_{i=0}^{N_{sq}-1} \frac{[s(i)]^2}{\sigma_N^2} \tag{38}$$

The constants K_{fm} and K_{mf} are selected at the time of system design so that the noise contribution to $a_P(i)$ can be neglected. The approximate signal power, SP, is given by

$$SP = \sum_{i=0}^{N_{sq}-1} [a_P(i)]^2 \tag{39}$$

$$= (K_{fm} \cdot K_{mf})^2 \sum_{i=0}^{N_{sq}-1} [s(i)]^2 \tag{40}$$

which is the signal energy over K_{mf} probe components.

(U) If the medium is stable over the measurement interval, the signal contribution to the $n(i)$ vector is zero. Thus, $\hat{n}(i)$ has a zero mean and a variance $K_{fm} \cdot K_{mf} \cdot \sigma_N^2$. Let

$$NP = \sum_{i=0}^{N_{sq}-1} [\hat{n}(i)]^2 \tag{41}$$

Then NP is χ^2 distributed with N_{sq} degrees of freedom. In the systems discussed here, $N_{sq} >> 50$ and the distribution on NP can be approximated by a Gaussian distribution with mean $N_{sq} \cdot K_{fm} \cdot K_{mf} \cdot \sigma_N^2$ and variance $2N_{sq} \cdot K_{fm} \cdot K_{mf}\sigma_N^2$. The mean-squared to variance ratio on NP is high, so NP is a good estimate of the noise power in K_{mf} probe components.

(U) The input signal-to-noise ratio, SNR_{in}, is defined as

$$SNR_{in} = \frac{\int s^2(t)dt}{\int n^2(t)dt} \tag{42}$$

where the integration is carried out over the probe measurement interval. From the sampling theorem,

$$\int s^2(t)dt = \frac{1}{2W} \sum [s(i)]^2 \tag{43}$$

$$\int n^2(t)dt = \frac{1}{2W} \sum [n(i)]^2 \tag{44}$$

where the summation extends over the $N_{mf} = N_{sq} \cdot K_{fm} \cdot K_{mf}$ samples in the probe measurement interval. Because the noise samples $n(i)$ are independent and have zero mean,

$$E\{\int n^2(t)dt\} = \frac{1}{2W} N_{sq} \cdot K_{fm} \cdot K_{mf}\sigma_N^2 \tag{45}$$

$$= \frac{1}{2W} (NP) \tag{46}$$

Similarly, the summation in Eq. (43) can be simplified if the channel is invariant over the measurement interval:

$$\frac{1}{2W} \cdot \sum s(i)^2 = \frac{1}{2W} \cdot K_{fm} \cdot K_{mf} \sum_{i=0}^{N_{sq}-1} [s(i)]^2 \tag{47}$$

$$= \frac{1}{2W} \frac{SP}{K_{fm} \cdot K_{mf}} \tag{48}$$

Substituting Eqs. (46) and (48) into Eq. (42) gives

$$SNR_{in} = \frac{1}{K_{fm} \cdot K_{mf}} \left(\frac{SP}{NP}\right) \tag{49}$$

Thus, the input signal-to-noise ratio can be determined from the probe measurements of SP and NP. Although this measurement is determined from the probe portion of the measurement

interval, it is also applicable to the information component by the assumed invariance of the medium.

C. INFORMATION COMPONENT PROCESSING

(C) The objective of the information component processing is to make correct decisions on the transmitted symbol values. These decisions can be scored against known answers in the case of a periodic transmission. For demonstration purposes, the received values can be printed as characters on a Teletype. In either situation, decisions are made on the basis of thresholds on the outputs of a matched filter.

1. Matched-Filter Operation

(C) The first step in the processing of the kth information component is to form a coherent average $a_I(k, i)$ of the information component:

$$a_I(k, i) = \sum_{j=0}^{K_{fm}-1} x[(2k+1)K_{fm} \cdot N_{sq} + jN_{sq} + i]; \quad 0 \leq i < N_{sq} \quad (50)$$

This yields a vector of N_{sq} points and is analogous to the computation of the $a_P(k, i)$ vector in the probe processing. The $a_I(k, i)$ vector contains K_{sf} information symbols, each composed of K_{sm} digits in a prescribed order. For the M5 and M6 experiments, $K_{sm}=3$ and $K_{sf}=5$, respectively.

(C) To match filter $a_I(k,i)$, a cross correlation is performed of $a_I(k,i)$ with $\hat{p}(l,i)$, where $\hat{p}(l,i)$ is the digit response found in the previous measurement interval, l. The decision process requires samples of the matched-filter output taken at intervals of one digit length, N_{dg}, apart. Thus, only K_{sq} cross correlations are needed to provide the required data from $a_I(k,i)$. Specifically, let

$$L'(k, j) = \sum_{i=0}^{N_{sq}-1} \hat{p}(i+jN_{dg}) a_I(k, i); \quad 0 \leq j < K_{sq} \quad (51)$$

where the index $i+jN_{dg}$ is taken *modulo* N_{sq}. The values $L'(k,j)$ represent a cross correlation of $a_I(k,i)$ with $\hat{p}(l,i)$ displaced by multiples of N_{dg} samples, or equivalently, T sec. Note that the cross correlation is performed in a circular manner, so that the overlap from one sequence period to the next is taken into account.

(C) A natural question arising from Eq. (51) is concerned with how much synchronization is required for the values $L'(k,j)$ to be taken at exactly the correct sampling time. *The answer is that no fine-grain synchronization is required.* If the $a_I(k,i)$ vector contains primarily the information component [and consequently the $a_P(k,i)$ vector contains primarily the probe component], as previously assumed, then $L'(k,j)$ is always taken at exactly the correct time. The reason for this is that the *transmission* provides a fixed time offset between the probe and information digits. This time offset is completely preserved in both sections of the processor. Thus, if probe digit A is separated from information digit B by m digits in the transmission, they will be separated by exactly m (*mod* K_{sq}) digits in the $a_P(k,i)$ and $a_I(k,i)$ vectors.

(C) The values $L'(k,j)$ are the response of a filter matched to the received digit, for each of the K_{sq} digits in the information frame. To make decisions on the information symbols, the response of a filter matched to each of the symbols must be obtained. Since the information symbols are formed from known combinations of digits, the symbol filter responses can be found from combinations of the $L'(k,j)$.

(C) Specifically, suppose that the jth symbol in the information component is as given in Eq. (19). Then output of the matched filter for the jth symbol in the kth frame, $L(k,j)$, is given by

$$L(k, j) = \sum_{i=0}^{K_{sm}-1} q(j, i) \sum_{m=0}^{N_{sq}-1} \hat{p}[l, (j \cdot K_{sm} + i)N_{dg} + m] a_I(k, m) \quad (52)$$

where the index $(j \cdot K_{sm}+i)N_{dg}+m$ is again taken *modulo* N_{sq}. The summation over m in the above equation is simply $L'(k, j \cdot K_{sm}+i)$, so the following result is obtained:

$$L(k, j) = \sum_{i=0}^{K_{sm}-1} q(j, i) L'(k, j \cdot K_{sm} + i) \quad (53)$$

Because the above equation is easily implemented, the use of variable symbol modulation places very little additional burden on the receiver processing.

2. Decision Process

(C) To determine the symbol values, a zero threshold is applied to the symbol matched-filter

outputs $L(k,i)$. If the filter output $L(k,i)$ is greater than zero, the decision $d(k \cdot K_{fs}+i)$ on the ith symbol in the kth information component is 1. Otherwise the decision is -1. In the M5 and M6 systems $K_{fs}=5$, so each information component yielded five bit decisions. These bit decisions were printed as a single five-level Teletype character during text transmissions.

(C) More elaborate decision techiques can be applied to reduce the effects of intersymbol interference. In the M5 and M6 systems, the choice of symbol durations was such that intersymbol interference was negligible, and these techniques were not required.

3. Scoring of Receiver Decisions

(U) To evaluate the system error performance, the receiver decisions $d(i)$ are scored against known correct values. This can be done as long as the symbol values in the information component are known, as they are in the case of a periodic transmission. The error count on the information components for the periodic transmission is designated E_I and is one of the parameters computed for every K_{mI} probe components.

(C) If information, unknown to the receiver, is being transmitted, it is of course not possible to score the information component. A completely adequate measure of system performance can be obtained, however, by performing the decision process on the vector $a_P(k,i)$ in a manner identical to that performed on $a_I(k,i)$. Since the digits in the probe have a fixed interpretation in terms of symbols, scoring of the probe component is always possible, since it is independent of the information being transmitted. The error count on the probe component is designated E_P.

(C) When a periodic transmission is sent, the expected values of the two error counts E_I and E_P should be the same, as the $a_P(k,i)$ and $a_I(k,i)$ vectors are statistically the same. On the other hand, when text is transmitted, E_I depends on the particular text transmitted, and it is not a measure of system error performance.

D. SYNCHRONIZATION

(C) In the preceding discussion, synchronization between the receiver and received signal has been assumed. When a periodic transmission is sent, the probe and information components are identical and no synchronization is necessary. On the other hand, when text is transmitted, synchronization is required to ensure that each component is processed in the correct manner.

(C) For a practical communication system, synchronization must be performed automatically and checked continuously. The systems considered here, however, were intended primarily to determine the feasibility of the coherent integration/matched-filter technique. Consequently, very little effort was expended on the synchronization problem. Indeed, during all of the performance measurement experiments a periodic transmission was carried out to eliminate the problem entirely. The following manual synchronization procedure was used whenever required for the actual transmission of text.

(C) Synchronization is achieved by interaction between an operator observing the oscilloscope display of $\hat{p}(k, i)$ and the processor. The operator can delay the processor time base for an integer number of digit durations by typing an appropriate command. Two steps are required to achieve synchronization with different transmission being required for each step.

(C) The first step requires the basic periodic transmission. The operator observes the display of $\hat{p}(k, i)$ and causes sufficient delays to locate the digit response in the center of the display. This locates the junction between the probe and information components to be within an integer number of sequence periods.

(C) During the second step, a transmission with a constant carrier in each information component is used. If the receiver is properly synchronized, the channel digit response is a clean pulse, with zero levels to either side. If the receiver is not properly synchronized, then the $a_P(k,i)$ vectors contain the carrier as well as the sequence, and the display of the digit response has a distinctive nonzero component. The operator delays the processor by multiples of T_{sq} until the proper display is obtained.

(C) The preceding procedure was taught to three operators who were unfamiliar with the total system operation. Each was able to synchronize the system within five minutes or so under conditions where the signal-to-noise ratio was 0 db. Synchro-

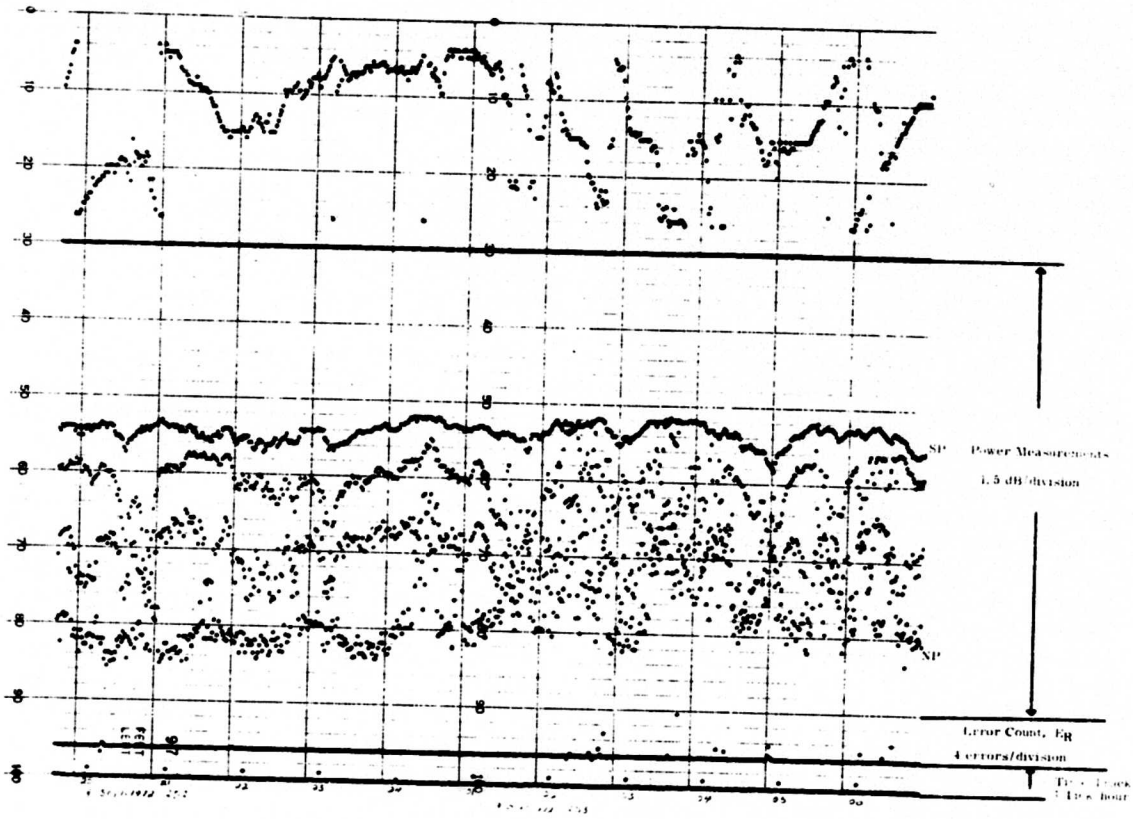

Figure 5. Typical multipoint plot from the M5 and M6 systems. (Figure unclassified.)

nization at lower signal-to-noise ratios is more difficult, but it can be done by an experienced operator.

E. IMPLEMENTATION

(U) The receiver processing for both communication systems was performed by small, general purpose, digital computers, frequently called minicomputers. The M5 systems were implemented on a Digital Equipment Corporation LINC-8 computer with a 4,096-word (12 bits/word) memory. The M6 systems were implemented on a DEC PDP-8E system with an 8,192 word (12 bits/word) memory.

(C) Both machines contained a hardware multiply capability. Such a feature is required if the system is to perform the matched filtering in real time. If it is assumed that both the information and probe components are match-filtered to receive the information and score the probe component, the number of multiplications, n_{mult}, required for either component is

$$n_{mult} = N_{eq} \frac{\text{multiplies}}{\text{matched filter}} \times K_{eq} \frac{\text{digits}}{\text{component}} \tag{54}$$

The time, T_{fm}, for a component is

$$T_{fm} = K_{fm} \cdot N_{eq} \frac{K_{cp}}{f_{clk}} \tag{55}$$

Thus, the multiplication rate, $\mathcal{R}_{mult}$, required is

$$\mathcal{R}_{mult} = \frac{n_{mult}}{T_{fm}} \tag{56}$$

$$= \frac{K_{eq} \cdot f_{clk}}{K_{fm} \cdot K_{cp}} \tag{57}$$

$$= 788 \text{ multiplications/sec} \tag{58}$$

for typical M5 and M6 experiment parameters. This rate is easily maintained with most modern minicomputers; however, the multiplication rate must nevertheless be considered in system parameter design.

(U) The primary output of the processor is digital magnetic tape—specifically, LINC format tape. The probe measurements and error counts are stored in blocks, with data from seven measurement intervals and time information in each block. One tape is filled every 6 or 7 days. Every time a tape block is written, an entry is typed into a Teletype log for verification purposes. A secondary, but important, output is given on a multipoint plotter controlled by the processor. This plot gives the values of SP and NP on a minute-by-minute basis. The probe error count, E_R, is also plotted, along with a timing track. Figure 5 depicts a typical multipoint plot and the associated scale factors.

IV. EXPERIMENTAL PROGRAM

(C) Five long-term experiments (M5A, M5B, M6A, M6B, and M6C) were performed between fixed sites in the Straits of Florida to evaluate the effectiveness of coherent integration/matched-filter techniques. The dates and durations for each of these experiments are shown in Table 1. A total of 4,554 hours (190 days) of valid data was obtained and analyzed over either 7- or 42-nmi distances. Section IVA describes the differences among the five experiments. Section IVB describes the experimental results.

A. DIFFERENCES AMONG EXPERIMENTS

(U) In each of the five experiments, the transmission was generated by the source off Fowey Rocks Light.* During the M5 experiment, signals were received at a hydrophone located 7nmi from the Fowey Rocks source, while in the M6 experiment, signals were received at the Bimini hydrophone, 42 nmi from the source. Each experiment had more than one part, as indicated by the third letter in the experiment identification; for example, M6C was the third part of the M6 experiment. The purpose of each part of both experiments is described below.

*(U) Reference 4 describes the fixed-site ranges in detail.

TABLE 2. *Common features of the M5A, M5B, M6A, M6B, and M6C experiments. (Table classified Confidential.)*

Center Frequency, f_o (Hz)	420
Nominal Bandwidth, W (Hz)	100
Modulation	Biphase
Format	Periodic, pseudorandom
# Digits/Sequence Period, K_{sq}	15
Symbol Modulation	Variable Symbol Modulation
# Digits/Symbol, K_{sm}	3
# Symbols/Frame, K_{fs}	5
# Sequence Periods/Frame, K_{fm}	4

(C) The M5 experiment had two parts, each having distinctly different purposes. The objective of the M5A experiment was to measure the communication system performance at low signal-to-noise ratios. Consequently, the transmitter power was reduced to give an average signal-to-noise ratio of 0 db. The resulting low signal-to-noise ratios increased the variance on the transmission measurements. After completion of the M5A portion, the signal power was increased for the second part of the M5 experiment to improve the quality of the transmission measurements. Because of the high input signal-to-noise ratios in the M5B experiment, the error rate was reduced to a point where system error performance could not be evaluated.

(C) The M6 experiment had three parts, each representing a different choice of system parameters. In the M6A experiment, the same transmission format was used as in the M5 experiment so as to obtain comparison data over the two distances. The sequence duration in this first experiment was known to be too short for reliable operation at the 42-nmi range. Further, the average signal-to-noise ratios at Bimini were lower than expected, because of inadequate source drive at Fowey Rocks. Consequently, a second experiment, M6B, with extremely high noise and multipath resistance (and low data rate) was initiated. Results from the M6B experiment indicated that its design was too conservative and that a compromise between the M6A and M6B parameters was in order. Subsequently, the third

TABLE 3. *Differences among experiments. (Table classified Confidential.)*

	M5A, M5B, M6A	M6B	M6C
Gross Characteristics:			
Digit Duration, T (ms)	19	67	33
Digit Waveshape	rectangular	(wideband,	coded)
Sequence Period, (ms)	286	1000	500
Symbol Duration, T_{sm} (ms)	57	200	100
Frame Component Duration, T_{fm} (ms)	1100	4000	2000
Processor Characteristics:			
A/D Compression Factor, K_{cp}	8	8	4
Samples/Digit, N_{dg}	4	14	14
Samples/Sequence Period, N_{sq}	60	210	210
Frames/Reference Determination, K_{mi}	32	16	16
Reference Determination Time (sec)	73	128	64
SNR_{in} Measurement Averaging Time (min)	8.5	14.9	7.5
Performance Characteristics:			
Probe processing gain (dB)	30	27	27
Symbol processing gain (dB)	17	22	19
Theoretical Minimum SNR_{in} for $p_e = .001$ (dB)	-7	-12	-9
Transmission Rate (bit/sec)	2.2	.63	1.25

experiment, M6C, was implemented as an optimized system for the 42-nmi distance.

(U) The five experiments have very similar transmission formats; indeed, the only major difference among the experiments is in the digit structure and duration. Table 2 depicts the parameters that were common to all experiments, but later paragraphs will point out the differences among the remaining system parameters. Because of the common features of the experiments and the software implementation of the processor, the transition from one experiment to the next was easily accomplished.

(U) Although five different experiments were performed, there are only three different sets of system parameters, with the M5A, M5B, and M6A experiments all employing the same transmission format. Table 3 gives the significant differences among the experiments.

(C) The primary difference between the M5A, M5B, and M6A format and the M6B and M6C format is in the digit duration and structure, with a digit in the M6B system being 3.5 times longer than a digit in the M5A system and a digit in the M6C system being 1.8 times longer than a digit in the M5A system. The purpose of the digit lengthening in the M6B and M6C systems was to increase the symbol processing gains and improve the performance against multipath.

(C) Of the last two systems, M6B and M6C, the M6B has the highest processing gains and, correspondingly, the lowest transmission rate. The M6C is exactly twice as fast and has 3 db less processing gain than the M6B system. Thus, the M6C system can be considered a compromise between the short digit durations of the M5A format and the very long durations of the M6B format.

(U) Both the M6B and the M6C systems employed broadband coding of the digit waveform to avoid the reduction of symbol bandwidth with the increase in symbol duration. This was necessary to retain the advantages of a broadband transmission against noise and multipath when the symbol duration is long relative to the digit bandwidth. A comparison of the digit spectra for

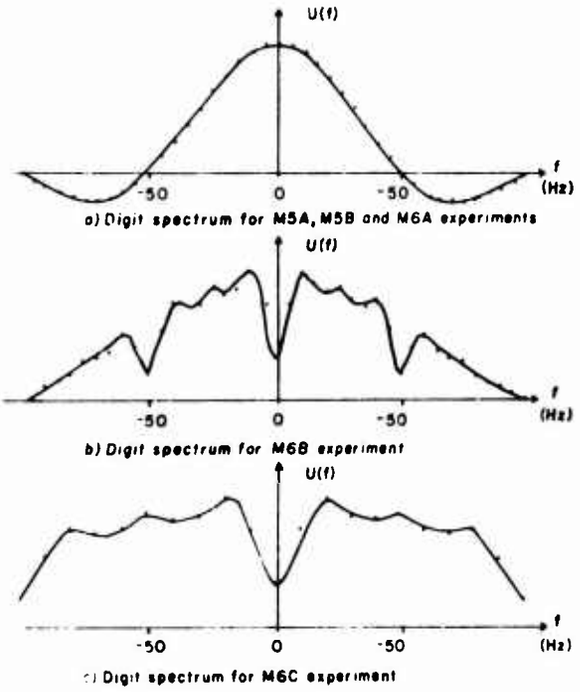

Figure 6. Comparison of digit spectra. (Figure unclassified.)

the three formats is shown in Figure 6. Because of the filtering of the source and reflector and the receiver analog filters, only the spectral components in a 100-hz band about the carrier are important.

8. EXPERIMENTAL RESULTS

(U) The five experiments yielded data on both acoustic transmission conditions and system error performance. In this section, only measurements that bear on the evaluation of system error performance or on future applications on the communication system are discussed. The remaining acoustic transmission measurements have been made available to other scientists, and they may be reported later.

1. Signal-to-Noise Ratio Histograms

(U) To interpret the communication performance data, an understanding of the signal and noise environment of each experiment is necessary. Figures 7 and 8 depict histograms of the wideband received signal-to-noise ratio, SNR_{in}, with ordinates of both frequency in percent and time in hours. The abscissa represents SNR_{in} averaged over the time interval shown in Table 3, and it

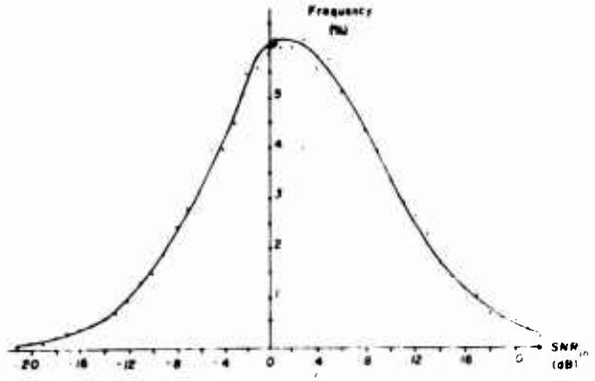

Figure 7a. Histogram of wideband received signal-to-noise ratio: M5A experiment. (Figure unclassified.)

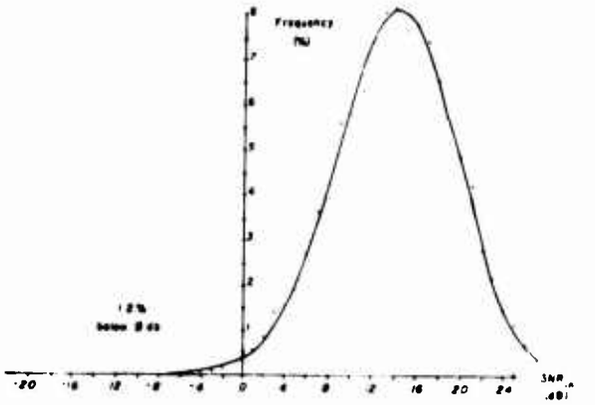

Figure 7b. Histogram of wideband received signal-to-noise ratio: M5B experiment. (Figure unclassified.)

is quantized in 1-db-wide bins. Because the source level was *not* held constant during the experiments, these histograms reflect only the signal-to-noise ratio environment as seen by the receiver, not a general measurement of acoustic propagation. Nevertheless, they indicate the extent of data available at a given input signal-to-noise ratio, so the statistical significance of the error measurements can be understood.

(C) Figure 7 gives the signal-to-noise ratio histograms for the two phases of the M5 series of experiments. As mentioned earlier, the source levels for the M5A experiment were deliberately reduced to achieve the low average signal-to-noise ratios shown in Fig. 7a. Consequently, a large amount of data with reasonably frequent errors was obtained in the M5A experiment.

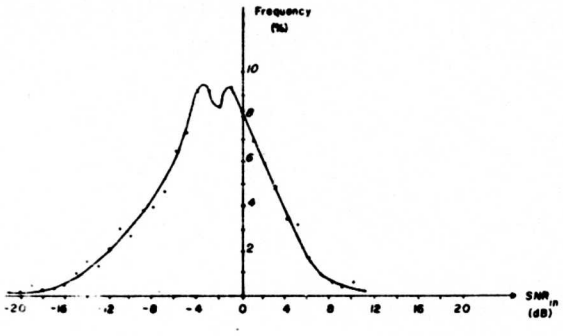

Figure 8a. Histogram of wideband received signal-to-noise ratio: M6A experiment. (Figure unclassified.)

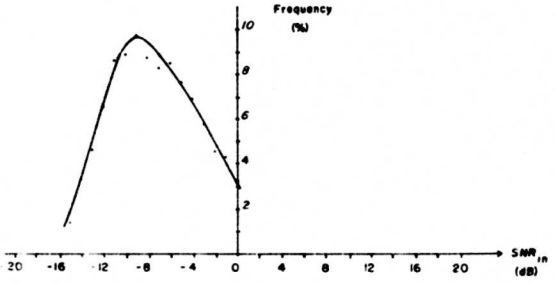

Figure 8b. Histogram of wideband received signal-to-noise ratio: M6B experiment. (Figure unclassified.)

Figure 7b gives the corresponding histogram for the M5B experiment, in which the source was driven at maximum available levels, yielding about a 12-db increase in mean SNR_{in} over that of the M5A experiment. Because only 1.2 percent of the M5B data correspond to SNR_{in} below 0 db, the error performance data for the M5B experiment were not statistically significant and were not processed further. Thus, the M5B experiment does not appear in the subsequent presentation of the error performance data.

(U) Figure 8 gives the SNR_{in} histograms for the three M6 series experiments. The M6A experiment was operated at signal-to-noise ratios that were only slightly (6 db) worse than those of the M5A experiment, so an adequate measurement of system performance could be achieved. Because of failure in an amplifier driving the Fowey Rocks source, very low signal-to-noise ratios were available for the M6B experiment, as shown in Fig. 8b.

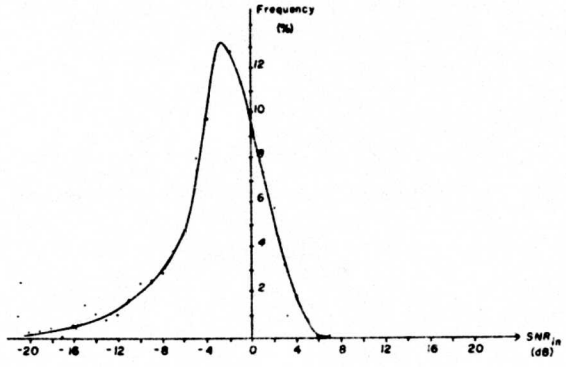

Figure 8c. Histogram of wideband received signal-to-noise ratio: M6C experiment. (Figure unclassified.)

These low signal-to-noise ratios motivated the choice of system parameters for the M6B experiment. Later, a new amplifier was installed at Fowey Rocks, which improved the signal-to-noise ratio situation at Bimini, and the M6C experiment was initiated. As shown in Fig. 8c, the M6C experiment experienced about the same SNR_{in} environment as the M6A experiment had experienced earlier.

2. Communication System Performance

(U) Evaluation of communication system performance is a difficult problem when one is confronted with the varying conditions of the acoustic medium. The technique described here is based on a well-known theoretical model, and it offers several advantages in terms of clarity and convenience.

(U) The primary data for the performance measurement consist of input signal-to-noise ratio averages and the cumulative error count $E = E_P + E_I$ taken over the averaging interval. Table 4 gives the averaging times and corresponding number of bit decisions for each experiment. Because the number of bit decisions is known, a probability of error for each data pair can be computed. A natural question arises as to the best way of presenting the relationship between average input signal-to-noise ratio and probability of error when thousands of such pairs are available.

(U) One method of evaluating the system performance would be to sum all of the error counts, E, for a fixed average signal-to-noise ratio and

TABLE 4. *Averaging times of SNR_{in} and bit decisions.* (*Table classified Confidential.*)

	M5A, M5B, M6A	M6B	M6C
SNR_{in} Averaging time (Min)	8.5	14.9	7.5
No. of bit decisions in averaging time	2205	1085	1085

then divide by the total number of bit decisions involved to obtain a probability of error. The disadvantage of this technique is that it does not indicate the variations in system error performance over time. To depict such variations, the error performance of each block is evaluated, with the results placed in histogram form to indicate the frequency of occurrence.

(U) A histogram of error probabilities would satisfy the above requirement; however, the nonuniformity of the probability scale makes the histogram difficult to understand. To overcome this problem, a conversion of the measured probability of error to a more uniform axis is helpful. A particularly helpful conversion from a systems analysis standpoint is to go from probability of error to output signal-to-noise ratio, which can be presented in decibels.

(U) Several alternatives exist for converting from error probability to output signal-to-noise ratio, but the simplest technique is to use a known relation from an existing theoretical model. In this paper, the conversion of probability of error to output signal-to-noise ratio is based on the classical results for the likelihood ratio receiver for a known linear, time-invariant channel with added white Gaussian noise. For this receiver, the probability of error, p_E, is given by

$$p_E = \Phi(-\sqrt{D}) \tag{59}$$

where

$$\Phi(u) = \int_{-\infty}^{u} (e^{-x^2/2})/\sqrt{2\pi}\, dx \tag{60}$$

and D is the output signal-to-noise ratio. For this situation, the conversion of error probability to output signal-to-noise ratio can be accomplished by solving Eq. (60) for D. That is

$$D = [\Phi^{-1}(p_E)]^2 \tag{61}$$

where $\Phi^{-1}(v)$ is the inverse of the function $\Phi(u)$ defined in Eq. (60). In the idealized situation of

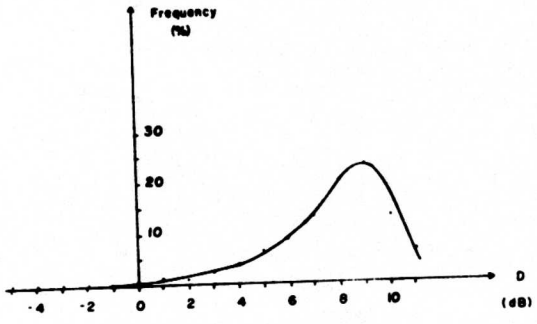

Figure 9a. Histogram of values of D: $SNR_{in} = -4$ db. (Figure classified Confidential.)

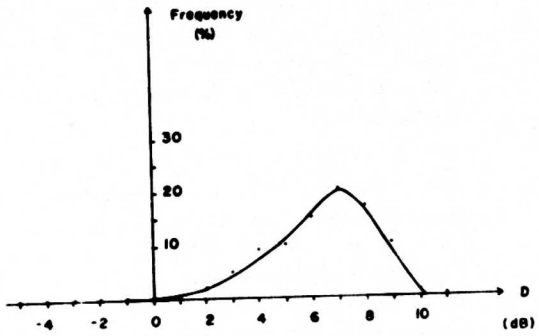

Figure 9b. Histogram of values of D: $SNR_{in} = -6$ db. (Figure unclassified.)

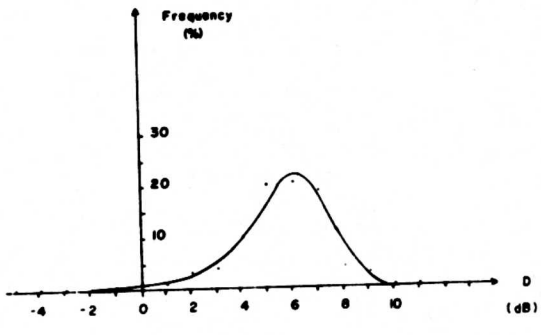

Figure 9c. Histogram of values of D: $SNR_{in} = -8$ db. (Figure unclassified.)

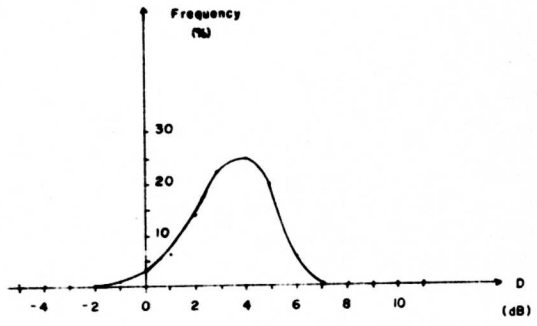

Figure 9d. Histogram of values of D: $SNR_{in} = -10$ db. (Figure unclassified.)

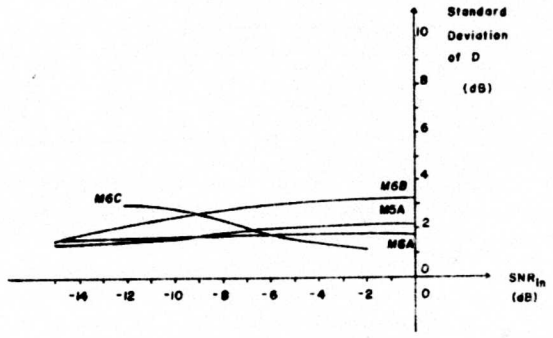

Figure 11. Standard deviation of D versus SNR_{in}. (Figure classified Confidential.)

the model, D is in fact the mean-squared-to-variance ratio of the matched-filter output. The motivation for the above choice of theoretical model comes from both its agreement with the assumed conditions of the real acoustic channel and its ease of use.

(U) The analysis technique from this point is straightforward. The error probability for each block of data is converted to output signal-to-noise ratio D in decibels through Eq. (61). Then, histograms of the resulting values of D are plotted for each signal-to-noise ratio. This provides a smooth and easily understood histogram, as shown in Fig. 9.

(U) One disadvantage of the histogram of output signal-to-noise ratios, D, is that the smallest measurable probability of error is about 0.001, which results from the fact that only one or two thousand bit decisions are made in each block. Such a probability of error corresponds to a value of D of about 11 db, so the histograms are necessarily truncated at that value.

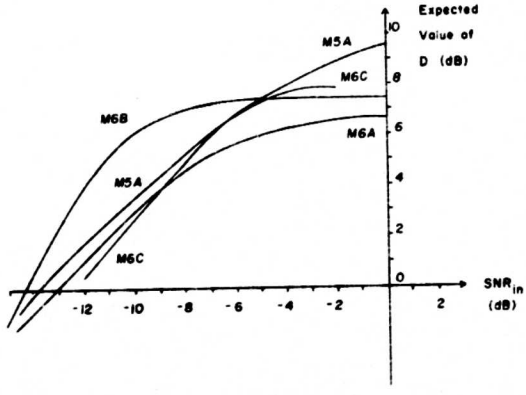

Figure 10. Mean D versus SNR_{in}. (Figure classified Confidential.)

(U) Figure 10 depicts the means of the output signal-to-noise histograms for the four communication experiments (M5B is omitted, because of its excessive signal-to-noise ratios). Points are shown on this plot only if at least 10,000 bit decisions were made at the given SNR_{in}. Consequently, each point shown is a statistically significant measure of the system performance. Figure 11 depicts the standard deviations of the same histograms.

(C) Note that there is a distinctive leveling off of output signal-to-noise ratio with increasing input signal-to-noise ratio. This is most likely due to the non-Gaussian nature of the noise, which becomes significant at higher signal-to-noise ratios. Also worthy of note is the fact that probabilities of error of 0.01 are achieved at input signal-to-noise ratios well below 0 db. Thus, a satisfactory system can be made to operate with SNR_{in} below 0 db. The leveling off of the M6B curve is probably due to the very long reference determination time involved (128 sec).

(C) Another way of interpreting communication system performance is to compare the experimental system performance with that of the idealized system described previously. For the

ideal system, the output signal-to-noise ratio D is given by

$$D_{ideal} = 2WT \cdot K_{fm} \cdot K_{am} \cdot SNR_{in} \qquad (62)$$

At a fixed SNR_{in}, the difference, η, between D_{ideal} and D can be found to indicate relative system performance:

$$\eta = \frac{D_{ideal}}{D} \qquad (63)$$

This has the advantage of placing systems with different transmission rates on the same basis. For example, the M6B system is better than the M6C system in absolute performance, because of its slower transmission rate. When compared relative to the ideal system with the same rate, however, the relative performance of the M6C system is better. This is shown in Fig. 12 for the four systems.

(C) Of the four systems shown in Fig. 11 the M5A system has the best relative performance, while M6B has the worst relative performance. This is probably because of the increased stability of the 7-nmi path with a 73-sec probe measurement interval over the 42-nmi path with a 128-sec probe measurement interval. Similarly, the relative performance of the M6A and M6C systems is worse than that of the M5A system strictly because of range. The relative performance difference between the M5A and M6C systems shown in Fig. 12 is not considered to be significant.

(C) In summary, the performance of the communication systems was very well established with large amounts of data. With careful choices of system parameters, a coherent matched-filter communication system such as M6C can yield error probabilities of 0.01 at input signal-to-noise ratios of −10 db. Such a system would be operating with a performance only 6 db worse than that of an idealized system.

3. Channel Stability Measurements

(C) The utility of the matched-filter technique studied here is highly dependent on the stability of the medium. If the acoustic channel changes significantly from the time of the probe measurement to the time of the information component processing, then the filter will not be properly

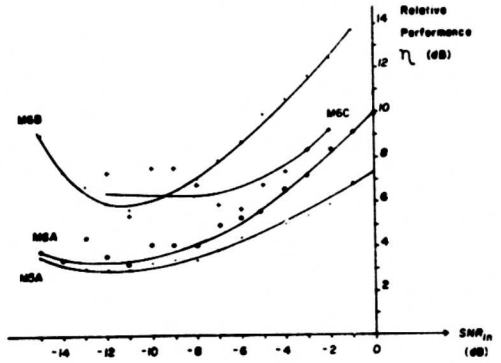

Figure 12. Mean η versus SNR_{in}. (Figure classified Confidential.)

matched and an increase in errors can be expected. On the other hand, if the acoustic medium is very stable, then the integration time of the probe component can be increased to improve the measurement of the channel digit response.

(U) Because of the importance of the channel stability to future applications, the five experiments included an elementary measurement of the wideband channel stability, specifically, the normalized cross correlation coefficient $\rho(k)$ described in Section IIIB. Although correlation coefficient data are available for the full duration of each experiment, only a few days of such data for each experiment have been analyzed. These days were chosen from continuous, high-quality data to determine any daily fluctuations. Only data with SNR_{out} greater than 10 db were considered.

(U) The most convenient way to understand the variations of the acoustic channel is to construct histograms of the correlation coefficient. Figure 13 depicts histograms of $\rho(k)$ for the M5A, M6A, and M6B experiments. The histograms represent one-day intervals (about 1,440 correlation values per histogram) with a bin size of 0.01. Note that the abscissa on each plot begins at 0.5, not zero. Since M5A and M6A used the same transmission parameters, the decrease in mean value can be attributed to the increased distance, 42 nmi instead of 7 nmi.

(C) Figures 13b and 13c depict the $\rho(k)$ histograms for the M6A and M6B experiments. The obvious widening of the M6B histograms is due to the

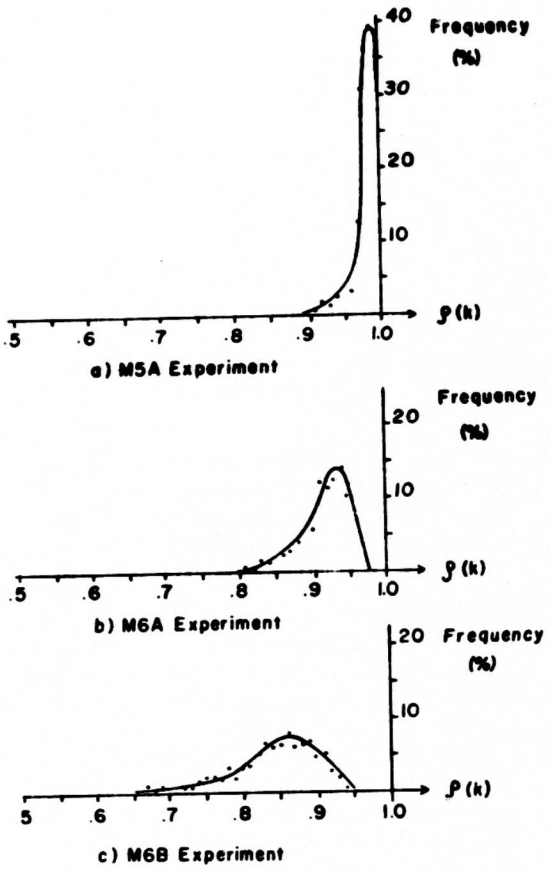

Figure 13. Histograms of $\rho(k)$. (Figure unclassified.)

increased measurement interval durations, 128 sec instead of 73 sec. The lower correlation values of the M6B experiment indicate that the measurement of the digit response is less accurate in the M6B system than in the M6A system. This offers at least a partial explanation for the poor relative performance of the M6B system shown in Figure 12. The correlation function histograms for the M5A and M5B experiments are nearly identical, as the distance and integration times are similar for the two experiments. Also, the histograms for the M6A and M6C experiments are similar.

V. SPATIAL STABILITY MEASUREMENTS

(U) The preceding sections described the operation and performance of an underwater acoustic communication system operating between two fixed points. In a practical submarine communication system, one or both ends of the acoustic channel is in motion, so spatial variations as well as temporal variations are important. This sections describes two measurements of the spatial stability of the medium and provides the foundation for the extension of the fixed-site communication techniques previously discussed to the submarine communication problem.

(U) The fixed-site experiments have shown the temporal stability of the medium to be sufficient to allow integration times of the order of one minute. From a purely geometric point of view, the medium should also be stable under spatial displacements that are common to submarine platforms. For example, a submarine on a 10-knot, zero Doppler track at a range of 100 nmi subtends less than 0.1 deg of arc in one minute. The wideband characteristics of the acoustic channel would not be expected to change significantly under such a displacement. Nevertheless, careful measurements have been made to validate this intuitive understanding.

(U) Two measurement techniques were employed to study the spatial stability of the acoustic channel. The first used coherent cross correlation of received waveforms without any coherent integration, and it yielded anomalous results. The second technique used coherent cross correlation with 13.4 db of coherent integration, and this produced consistent results. In the following sections, each measurement technique is described in detail, and an explanation of the differences in their results is offered.

A. COHERENT CROSS CORRELATION WITHOUT COHERENT INTEGRATION

(U) In this measurement technique, the spatial stability of the medium was measured in terms of normalized correlation coefficients, $\rho_1{}^*(i)$, analogous to the correlation coefficient, $\rho(k)$, studied in the M5 and M6 experiments. Because of the presence of the Doppler effect, however, the definition had to be modified slightly.

(U) The transmission was a 15-digit, pseudorandom sequence similar to that of the M5A, M5B, and M6A experiments. The sequence was scaled from the previous carrier frequency of 420 hz to a center frequency of 350 hz, to be com-

patible with the acoustic source. The resulting sequence has a period T_{sq} of 343 msec and a zero-to-zero bandwidth of 87.5 hz. and it was transmitted continuously from the towed source during each experiment.

(U) Let $x_1(t)$ be the received signal, bandpass-filtered in a 100-hz band centered on the carrier frequency of 350 hz. Consider a segment of $x_1(t)$ of duration T_{sg} that contains an integer number of sequence periods at zero Doppler, that is, $T_{sg}=kT_{sq}$ for some integer k. The normalized cross correlation function $\rho_1(\tau)$ of this segment with the input $x_1(t)$ is given by

$$\rho_1(\tau)=\frac{\int_{t_0}^{t_0+T_{sg}} x_1(t)x_1^*(t+\tau)dt}{\sqrt{\int_{t_0}^{t_0+T_{sg}} |x_1(t)|^2dt \int_{t_0+\tau}^{t_0+T_{sg}+\tau} |x_1(t)|^2dt}} \quad (64)$$

where t_0 is the starting time of the selected segment. Note that, in general, $\rho_1(\tau)$ is complex valued. If there is no Doppler and the medium is perfectly stable, then $\rho_1(\tau)$ will be periodic, with the same period as the sequence, and it will attain a maximum value of unity. If there is no Doppler, but the medium is changing, values of $\rho_1(\tau)$ taken at multiples of the sequence period are a measure of the stability of the channel. Consequently, the correlation function evaluated at multiples of the segment duration $\rho_1(iT_{sg})$, $i=1, 2 \ldots$, will also be an indication of channel stability.

(U) Since $x_1(t)$ was generated by a moving source, the effects of Doppler will be present, even on a nominal "zero Doppler" track. A convenient approach to understanding the effects of Doppler is to consider it as producing either a time compression or expansion of the received signal. Let T_{sg} be the duration of a segment of $x_1(t)$ at zero Doppler and let T'_{sg} be the duration of the same segment as received from the source approaching the hydrophone at a velocity v. Then

$$T'_{sg}=(1-v/c)T_{sg} \quad (65)$$

where c is the average speed of sound in the same units as v. If the source is approaching the receiver at 10 knots, T_{sg} is reduced by 0.34 percent. Similarly, if the source is leaving the receiver at 10 knots, T_{sg} will be increased by 0.34 percent. Although the percent variation may appear to be small, the consequences of such time-axis distortions are significant when coherent techniques are employed.

(U) If the velocity of the source and the average sound velocity were known, the normalized correlation function of Eq. (64) could be evaluated at multiples of the Doppler-distorted sequence duration, T'_{sg}. Unfortunately, neither variable is sufficiently well determined to calculate T'_{sg} adequately. In the September 1973 experiments, a new correlation coefficient, $\rho_1^*(i)$, was defined so as to alleviate the effects of Doppler. Let,

$$\rho_1^*(i)=\max |\rho_1[iT_{sg}(1-u)]|; \quad -l\leq u\leq +l \quad (66)$$

where $i=1 \ldots 7$.

$$l=\frac{|v^*|}{c_{est}} \quad (67)$$

v^* is the largest anticipated Doppler rate and c_{est} is an estimate of the average speed of sound. The purpose of selecting the maximum magnitude of $\rho_1(\tau)$ in an interval is to ensure that the correlation coefficient corresponds to the correlation value at correct time alignment in the presence of Doppler.

(U) Two important differences between the correlation coefficient $\rho(k)$ of the M5 and M6 experiments and the correlation coefficients $\rho_1^*(i)$ of the September 1974 experiment must be noted. First, in the M5 and M6 experiments, $\rho(k)$ was derived from a cross correlation of two coherently integrated waveforms $\hat{p}(k,i)$, $\hat{p}(k-1,i)$ in Eq. (36) [whereas $\rho_1^*(i)$ is derived from a cross correlation of two unintegrated input waveforms, $x_1(t)$, $x_1(t+\tau)$ in Eq. (64)]. Consequently, the coefficients $\rho_1^*(i)$ are much more sensitive to both noise and short-term channel variations than the coefficient $\rho(k)$ measured previously.

(U) The second important difference between the measurement of $\rho_1^*(i)$ in the September 1974 experiment and the measurement of $\rho(k)$ in the M5 and M6 experiments is that $\rho_1^*(i)$ is insensitive to pure time shifts in the medium. That is, $\rho_1^*(i)$ can be close to unity for a medium exhibiting rapid changes in time delay because of the maximization included in the definition of $\rho_1^*(i)$. Fortunately, many previous transmission measurements have shown that such changes do not exist in the ocean acoustic medium.

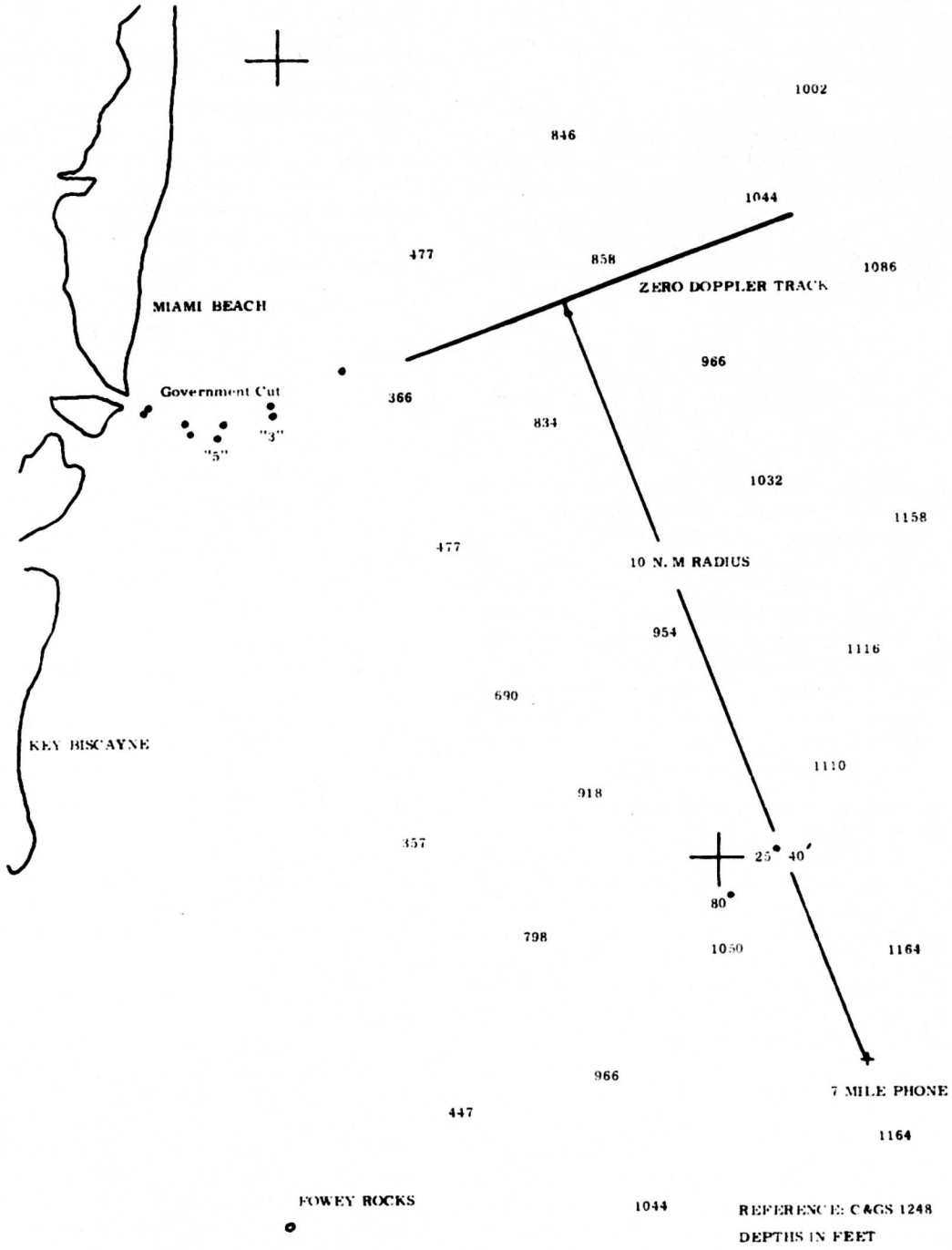

Figure 14. Vessel track for the September 1973 experiments. (Figure unclassified.)

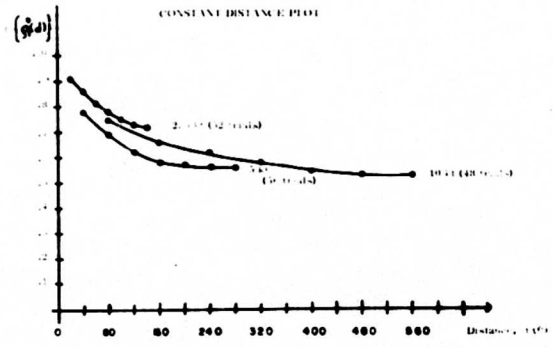

Figure 15a. Average correlation coefficients versus spatial displacement, Sept. 14, 1973. (Figure unclassified.)

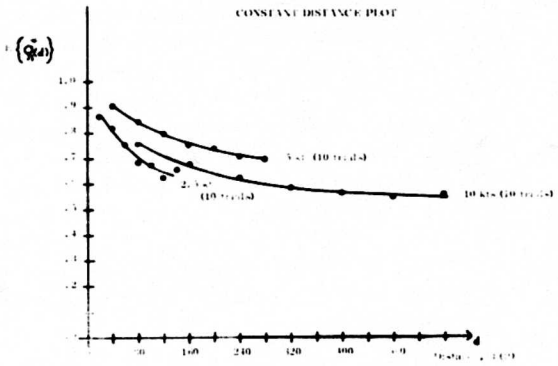

Figure 15b. Average correlation coefficients versus spatial displacement, Sept. 21, 1973. (Figure unclassified.)

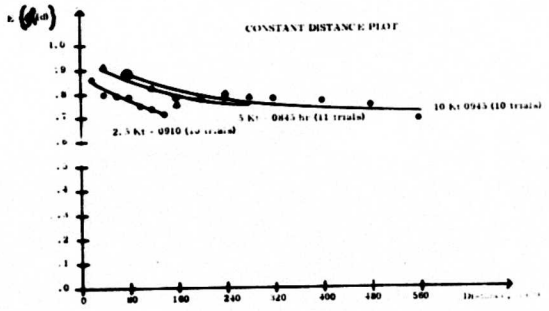

Figure 15c. Average correlation coefficients versus spatial displacement, Sept. 25, 1973. (Figure unclassified.)

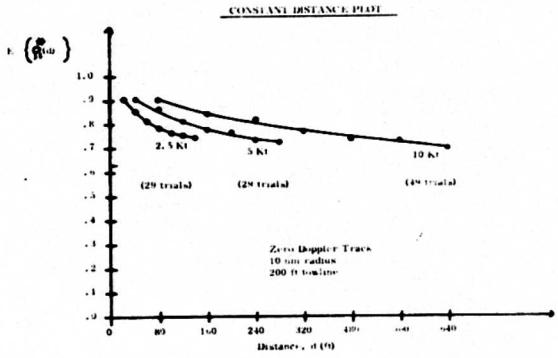

Figure 16. Averages of average correlation coefficients versus spatial displacement. (Figure unclassified.)

(U) The preliminary spatial stability measurements were conducted with a towed HX90 source in the Straits of Florida during September 1973. Figure 14 depicts the vessel track during these experiments. The source was towed at approximately 200-ft depth with vessel speeds of 2.5, 5, and 10 knots. Signals from the source were received at a hydrophone approximately 7 nmi from the Fowey Rocks Light and were sent via cables to the laboratory on shore.

(U) Figure 15 depicts the average correlation coefficients obtained during three experiments in September 1973. Here $T_{ss}=5$ sec and i ranges from 1 to 7, corresponding to a 40-sec maximum extent. The coefficients $\rho_1^*(i)$ are plotted as a function of distance, not time, so as to indicate the stability for a fixed spatial displacement, independent of source velocity. Because only 40 sec of data could be processed, the spatial variations are measured over shorter displacements for lower source velocities. Data for which $\rho_1^*(i)<0.8$ have been eliminated from the plot, as such a value is indicative of an inadequate signal-to-noise ratio.

(U) The data given in Fig. 15 exhibit several obvious anomalies. First, the values of the correlation coefficients do not agree for the same spatial displacement. If these correlation coefficients actually measured the spatial variations of the medium, coefficients corresponding to the same spatial displacement should be equal, which is not the case. Second, on different days the relative positions of the curves for different source speeds change. For example, on September 14, the 2.5-knot data were the most stable, whereas on September 21 and 25 the 2.5-knot data were the

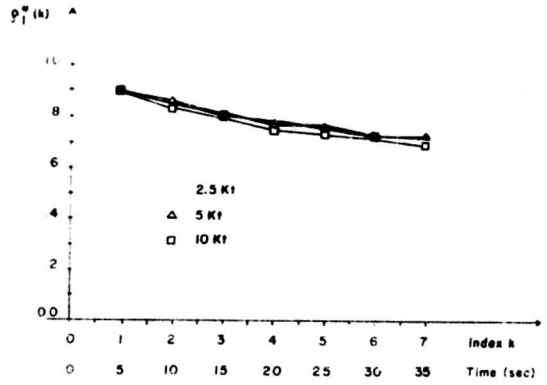

Figure 17. Averages of average correlation coefficients versus time displacement. (Figure unclassified.)

least stable. Similarly, the relative positions of the 5- and 10-knot runs change from one day to the other.

(U) Figure 16 gives the average of the results depicted in Figs. 15a, 15b, and 15c. As in the one-day plots, the correlation coefficients do not appear to depend on spatial displacement. Further, the correlation coefficients are smaller for low source speeds than for higher source speeds. Neither result agrees with common sense.

(U) In Fig. 17 the average correlation coefficients of Fig. 16 are plotted as a function of time displacement instead of spatial displacement. The close agreement between the curves for different source speeds is apparent. This indicates that the correlation coefficients $\rho_1^*(i)$ are dependent on time displacement, not spatial displacement as originally intended. Also, the time stability is drastically reduced from the values obtained in the extensive fixed-site experiments (M5 and M6), where correlation coefficients of 0.9 were obtained over longer intervals (73 and 64 sec.).

(U) Because of the above anomalies in the data, a search for possible explanations was initiated. A brief study was made of a cw transmission from the towed source to determine any peculiarities in the source motion. This study showed that variations of the source about its intended linear track were insignificant.

(U) The most probable causes of the anomalies in the data are noise and surface modulation. Although the signal-to-noise ratio during each experiment was estimated to be in excess of 10 db, no quantitative measurement such as those in the M5 and M6 experiments was available. Because no coherent integration was used, the correlation coefficients $\rho_1^*(i)$ are particularly sensitive to noise. Although previous measurements in the Straits have indicated that the extent of surface modulation is insufficient by itself to account for the observed results, surface modulation would also reduce the values of the correlation coefficients. Both of these effects are independent of spatial displacement, and they vary in extent on a day-by-day basis, which is in agreement with the data obtained.

(U) Although the experiments described in this section were unsuccessful in measuring the spatial stability of the medium, the lesson learned is important. That lesson shows the importance of substantial coherent integration in the measurement of medium stability, so the effects of noise and surface modulation do not influence the stability measurement. As a result of the September 1973 experiment, a second measurement technique employing coherent integration was developed, and this yielded a valid measurement of spatial stability.

B. COHERENT CROSS CORRELATION WITH COHERENT INTEGRATION

(U) After the preliminary spatial stability measurements in September 1973, development of a measurement technique including coherent integration was initiated. The requirement for coherent integration was based on two considerations. First, the September 1973 experiments showed that noise and surface modulation precluded measurement of the spatial stability when no coherent integration was used; and second, an opportunity to study spatial stability at long ranges in the deep ocean was available. The input signal-to-noise ratio at these ranges required coherent integration to obtain adequate representation of the signal. The resulting measurement technique, which employs coherent cross correlation with coherent integration, is described below.

(U) Because of the need to perform coherent integration as well as to accommodate Doppler effects, fast Fourier transform techniques (FFT) were employed. These techniques provided two

constraints on the measurement process. First, the coherent integration time was limited to about 30 sec because of the memory limitations of the processing equipment. Second, the transmission format was selected to have an integer number of sequence periods contained in the transform interval, so that a close alignment of the signal and FFT spectral lines would be obtained. Once these two constraints were satisfied, the application of FFT techniques allowed straightforward measurement of both the spatial stability and the input signal-to-noise ratio.

(U) The transmission for the experiment was a 31-digit linear, maximal sequence with 15 carrier cycles per digit. Modulation of the 350-hz carrier was accomplished by complementary phase techniques, so as to yield a high-level carrier and yet retain a higher total power than with amplitude modulation. The transmission is given by

$$m(t)=\sum_{-\infty}^{+\infty}\{a(i)\cos 2\pi f_0 t+[1-a(i)]\sin 2\pi f_0 t\}\times\{U(iT)-U[(i+1)T]\} \quad (68)$$

where $f_0=350$ hz is the carrier frequency, $T=0.042857$ sec is the digit duration, $\{a(i)|a(i)\in\{0,1\}\}$ are the AM sequence coefficients, and $U(t)$ is the unit step function. This transmission has the same power spectrum as an amplitude-modulated sequence of the same structure, but it has approximately 3 db higher total power. Because $m(t)$ is periodic, with a period of 1.329567 sec, its spectrum has a line spacing of 0.752125 hz. The transmission has a zero-to-zero bandwidth of 46.667 hz, determined by the digit duration, T.

(U) After initial analog bandpass filtering to a 50-hz band about 350 hz, the received signal $s_1(t)$ is sampled at a rate of $4f_{rec}$ where f_{rec} is the receiver center frequency ($f_{rec}=350$ hz for zero Doppler). The resulting samples were compressed in the manner defined in Eqs. (26) and (27), but with $K_{cp}=10$. This reduces the number of samples to agree with the sampling theorem requirements and yields 186 compressed samples per sequence period. For convenience in the subsequent discussion, these samples are considered in terms of 2,048 long, complex vectors, $\{Z(k, i)|i=0 \ldots 2{,}047\}$, where the k indicates the kth transform interval. That is, the sample following $Z(k, 2{,}047)$, is $Z(k+1, 0)$, and so forth.

(U) An input vector of 2,048 complex samples $Z(k, i)$ contains approximately 22 sequence periods of the transmission at zero Doppler. Specifically, the 2,048 complex samples correspond to a 29.257143-sec time interval, whereas 22 sequence periods occupy 29.228474 sec, a 0.1 percent difference. Consequently, the spectral lines of a 2,048-complex-point FFT will very nearly align with the signal spectral lines. The actual offset between the ith signal line from the carrier and the corresponding transform line, $\delta_{FFT}(i)$ is given by

$$\delta_{FFT}(i)=\left(\frac{1}{1.329567}-\frac{22}{29.257143}\right)i \quad (69)$$

$$=0.000728i \text{ hertz} \quad (70)$$

For the energetic lines near the carrier, this offset is less than half the FFT line spacing of 0.034180 hz, and it will be neglected in the subsequent discussion.

1. Operation at Zero Doppler

(U) To understand the operation of the measurement technique, first consider its operation with zero Doppler. Because the transform interval contains nearly 22 sequence periods, every 22nd transform spectral line from the carrier will contain signal energy. The intervening 21 transform lines will contain only noise energy. Consequently, a processing gain of 22 (13.4 db) can be achieved by considering only every 22nd transform spectral line about the carrier.

(U) Let $\{Z(k, i)|-1{,}024\leq i\leq 1{,}023\}$ be the discrete Fourier transform of the input vector $\{z(k, i)|i=0 \ldots 2{,}047\}$ with the i index on $\{Z(k, i)\}$ selected so the $Z(k, 0)$ corresponds to the carrier line at zero Doppler. Define a new spectrum $\{S(k, i)|-32\leq i\leq 31\}$ from $\{Z(k, i)\}$ by selecting every 22nd spectral line of $\{Z(k, i)\}$ as follows:

$$S(k, i)=Z(k, 22\cdot i); \quad -32\leq i\leq 31 \quad (71)$$

From the discussion of the preceding paragraph, $\{S(k, i)\}$, will contain signal energy with a 13.4-db improvement in signal-to-noise ratio over that of $\{Z(k, i)\}$, because of the elimination of 21 lines containing noise alone.

(U) The measurement of spatial stability is accomplished by calculating the normalized cross

correlation coefficient, $\rho_2^*(i)$, between the signal waveform in the kth transform interval with that of the $(k-1)$th transform interval. Let $s(k, i)$, $i=0 \ldots 127$, be the inverse discrete Fourier transform of the kth signal spectrum $S(k, i)$. The normalized cross correlation function $\rho(k, j)$ between $s(k, i)$ and $s(k-1, i)$ is defined by

$$\rho(k, j) = \frac{\sum_{i=0}^{127} s(k, i)s(k-1, i+j)}{\sqrt{\sum_{i=0}^{127} |s(k, i)|^2 \sum_{i=0}^{127} s(k-1, i)|^2}} \quad (72)$$

where the $(i+j)$ index is taken *modulo* 128 so that $\rho(k,j)$ is the result of a circular correlation. Because the transform length is not an exact multiple of the sequence period, $\rho(k,0)$ does not give the correlation corresponding to exact alignment between the two waveforms. Consequently, a maximization process must be performed to determine the correlation coefficient, $\rho_2^*(k)$, which represents the medium spatial stability:

$$\rho_2^*(k) = \max |\rho(k, j)|; \quad 0 \leq j \leq 63 \quad (73)$$

The coefficient $\rho_2^*(k)$ has the same ambiguity in terms of pure time shifts that the $\rho_1^*(i)$ coefficients had in the preliminary experiments. As before, this ambiguity is known to be insignificant, on the basis of other experimental data.

(U) To properly interpret the correlation coefficient, $\rho_2^*(k)$, a quantitative knowledge of the signal-to-noise ratio of both the $S(k, i)$ and $S(k-1, i)$ vectors is needed. The signal power $SP(k)$ can be computed directly from the signal spectrum $S(k,i)$.

$$SP(k) = \sum_{i=-32}^{31} |S(k, i)|^2 \quad (74)$$

To determine the noise power, the power in a transform spectral line in between the signal lines is calculated.

$$NP(k) = \sum_{i=-32}^{31} |Z(k, 22i+11)|^2 \quad (75)$$

If it is assumed that the noise is white (at least relative to the signal line spacing of 0.752691 hz), $NP(k)$ gives a measure of the noise content of $S(k, i)$. Consequently, the signal-to-noise ratio $SNR_{out}(k)$ of $S(k, i)$ is simply the ratio of $SP(k)$ to $NP(k)$

$$SNR_{out}(k) = \frac{SP(k)}{NP(k)} \quad (76)$$

The input signal-to-noise ratio $SNR_{in}(k)$ is 22 times (13.4 db) worse than $SNR_{out}(k)$.

$$SNR_{in}(k) = \frac{1}{22} SNR_{out}(k) \quad (77)$$

Thus, both the input and output signal-to-noise ratios can be quantitatively measured in each transform interval

2. Operation with Nonzero Doppler

(U) Measurement of the correlation coefficient $\rho_2^*(k)$ and the input and output signal-to-noise ratios is not significantly more difficult when the Doppler is nonzero. Let f_0' be the Doppler-shifted carrier frequency

$$f_0' = \frac{f_0}{1-v_r/c} \quad (78)$$

If the difference between f_0' and the receiver center frequency, f_{rec}, is small, then the effect of Doppler on the received signal is approximately a frequency translation. Such a frequency translation acts as a fixed offset between the zero-Doppler location of the signal spectral lines and the actual received spectral lines.

(U) Consider the situation where f_0' and f_{rec} differ by Δf hz.

$$\Delta f = f_0' - f_{rec} \quad (79)$$

Then if the effects of Doppler are considered as a frequency translation, the signal spectrum will be displaced by r' transform spectral lines.

$$r' = \frac{\Delta f}{0.034180} \quad (80)$$

In general, the displacement r' will not be an integer. The integer offset, r^*, to the *closest* transform spectral line can be found from

$$r^* = [r' + 0.5] \quad (81)$$

where the square brackets $[x]$ indicate the greatest integer part of x. In subsequent discussion, r^* is called the vernier frequency index.

(U) Given the vernier frequency index, r^*, Eq. (71) for the signal spectrum can be modified to incorporate the effects of Doppler:

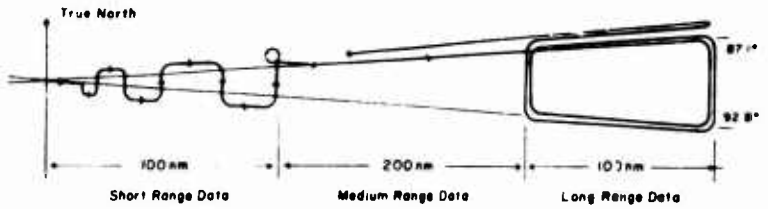

Figure 18. Vessel track for the January 1974 experiment. (Figure unclassified.)

$$S(k, i) = Z(k, 22i + r^*) \tag{82}$$

Similarly, Eq. (75) for the noise power becomes

$$\mathrm{NP}(k) = \sum_{i=-32}^{+32} |Z(k, 22i + 11 + r^*)|^2 \tag{83}$$

With these two modifications of the zero-Doppler equations, the derivation of the correlation coefficient $\rho_2^*(k)$ and the signal-to-noise ratios remain valid in the presence of Doppler.

(U) The significant remaining problem is the determination of the vernier frequency index, r^*, by the measurement system. One approach is to search the received signal spectrum $Z(k, i)$ for the largest signal line (presumably the carrier at f_0' hz) and calculate Δf and r^*. Unfortunately, selective fading due to multipath will occasionally reduce the carrier level below that of the adjacent sidebands and the system will obtain an incorrect value for r^*.

(U) To avoid this problem, the measurement system determined r^* on the basis of broadband signal-to-noise ratio. Specifically, the following quantity is calculated

$$\mathrm{SNR}_{\mathrm{out}}(k, r) = \frac{\sum_{i=0}^{63} |Z(k, 22i + r)|^2}{\sum_{i=0}^{63} |Z(k, 22i + r + 11)|^2} \tag{84}$$

for $-10 \le r \le 11$. The expression $\mathrm{SNR}_{\mathrm{out}}(k, r)$ given in Eq. (84) is simply the output signal-to-noise ratio if r were the correct vernier frequency index. The range of r is constrained to be within one signal-line separation (0.752691 hz, or approximately a 6.4-knot Doppler uncertainty), as $\mathrm{SNR}_{\mathrm{out}}(k, r)$ will be periodic because of the regular spacing of the signal spectral lines. In actual measurements, the receiver frequency, f_{rec}, is adjusted to be within about 0.1 hz of f_0', so this constraint in r is not a problem.

(U) To determine the value of r^*, the processor selected the value of r that yielded the highest value of $\mathrm{SNR}_{\mathrm{out}}(k, r)$. Because $\mathrm{SNR}_{\mathrm{out}}(k, r)$ is based on the broadband signal spectrum and not on any single spectral line, the resulting frequency offset, r^*, is not disturbed by selective fading. Given r^*, the calculation of $\rho_2^*(k)$ and the signal-to-noise ratios is easily accomplished. Indeed, the measurement system performed all necessary calculations in real time, producing new values of $\rho_2^*(k)$ and $\mathrm{SNR}_{\mathrm{out}}(k)$ every 29.257143 sec.

3. *Experimental Results*

(U) During January 1974, the HX90 acoustic source was towed in the deep ocean between Eleuthera and Bermuda. The approximate vessel track relative to the hydrophone is shown in Fig. 18. Signals from the source were received at a fixed hydrophone and processed with the coherent integration technique described above. The ranges of the experiment varied from 0 to 400 nmi, with most of the experiment being conducted at ranges between 300 and 400 nmi. During the experiment, the vessel speed was maintained at approximately 6 knots.

(U) The digital processor was in nearly continuous operation during the 12 days of the experiment, yielding correlation coefficients $\rho_2^*(k)$ and signal-to-noise ratios every 29.257143 sec. These and other results were recorded on digital magnetic tape and simultaneously plotted on a multipoint recorder. Figure 19 depicts an annotated typical multipoint plot from the processor. As in the M5 and M6 experiments, this plot was an important aid in maintaining quality control during the experiment.

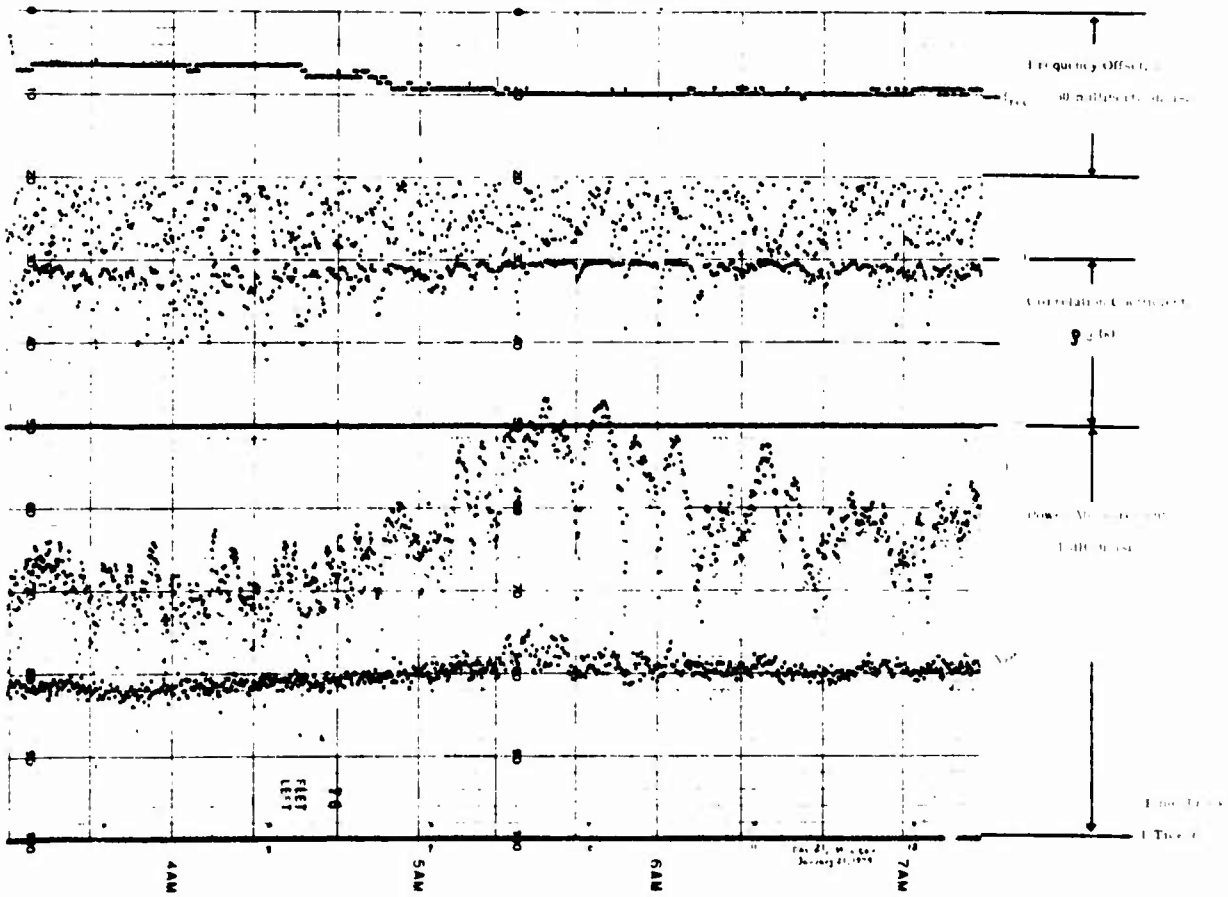

Figure 19. Typical multipoint plot from the January 1974 experiment. (Figure unclassified.)

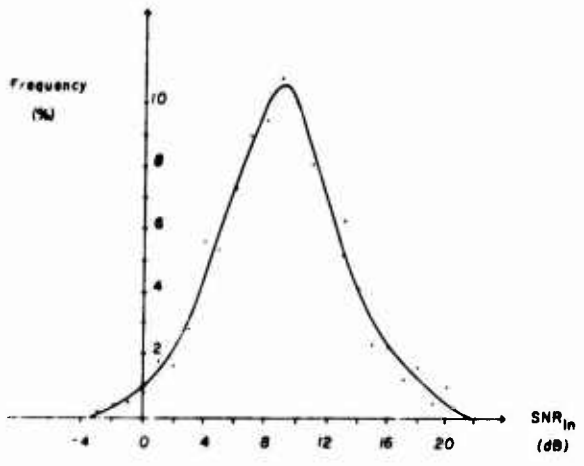

Figure 20a. Histogram of SNR_{in} from the January 1974 experiment: short-range data. (Figure unclassified.)

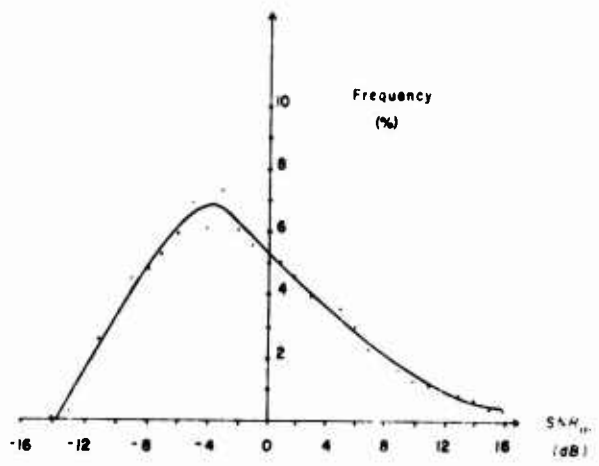

Figure 20b. Histogram of SNR_{in} from the January 1974 experiment; medium-range data. (Figure unclassified.)

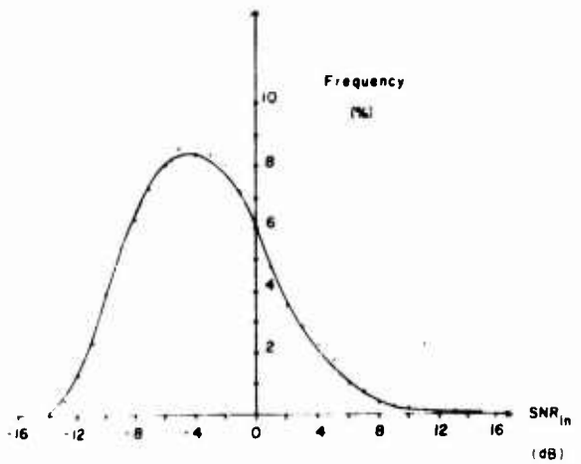

Figure 20c. Histogram of SNR_{in} from the January 1974 experiment: long-range data. (Figure unclassified.)

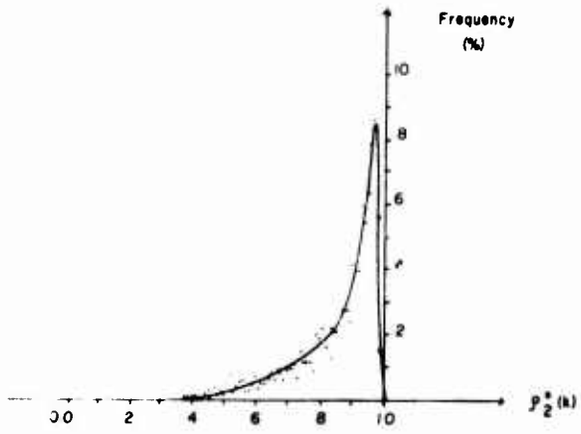

Figure 21a. Histogram of $\rho_2^*(k)$: short-range data. (Figure unclassified.)

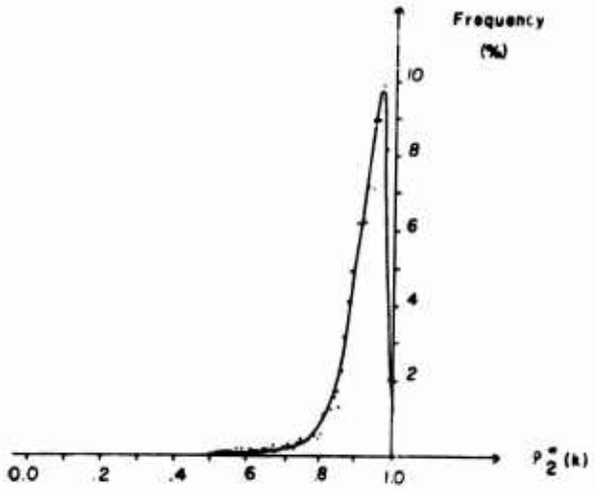

Figure 21b. Histogram of $\rho_2^*(k)$: medium-range data. (Figure unclassified.)

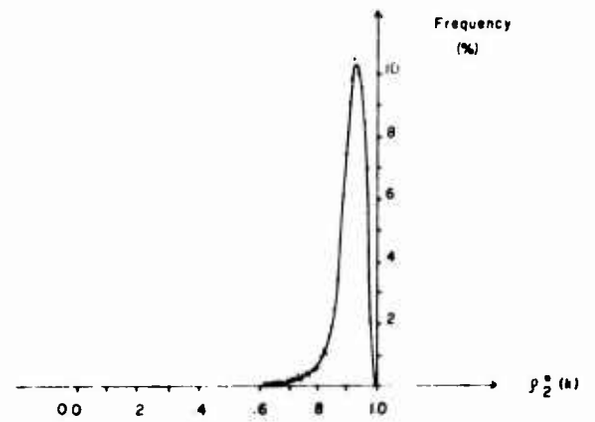

Figure 21c. Histogram of $\rho_2^*(k)$: long-range data. (Figure unclassified.)

(U) Data from the January 1974 experiment can be divided into three sets. The first set, called the "short range," includes data in which the source was going from 0 to 100 nmi. The second set, called the "medium range," includes data in which the source was going from 100 nmi to 300 nmi. Because of the severe range changes, data in these two sets represent measurements over a wide variety of transmission conditions. The third set, which is the largest, includes the data taken at ranges between 300 and 400 nmi and is referred to as the "long range" data. No correction for changes in range has been applied to any of the three data sets.

(U) Figure 20a depicts a histogram of the received signal-to-noise ratio in decibels for the short-range data. The mean signal-to-noise ratio is 9.6 db, with a standard deviation of 4.3 db. Figure 20b depicts an analogous histogram for the medium-range data. For the medium-range data the mean signal-to-noise ratio is −0.9 db, with a standard deviation of 6.2 db. Figure 20c depicts a histogram for the long-range data with a mean of −3.0 db and a standard deviation of 4.4 db. The reduced standard deviation for the long-range data as opposed to the medium-range data is due to the relative uniformity of the long-range data in terms of transmission conditions.

(U) Spatial stability was evaluated by means of

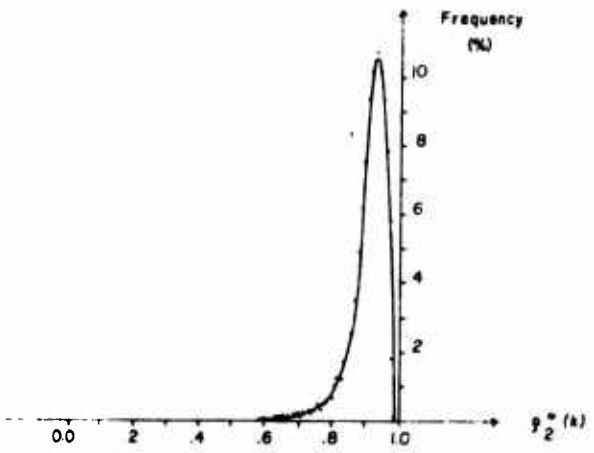

Figure 22a. Histogram of $\rho_2^*(k)$ values for full Doppler conditions. (Figure unclassified.)

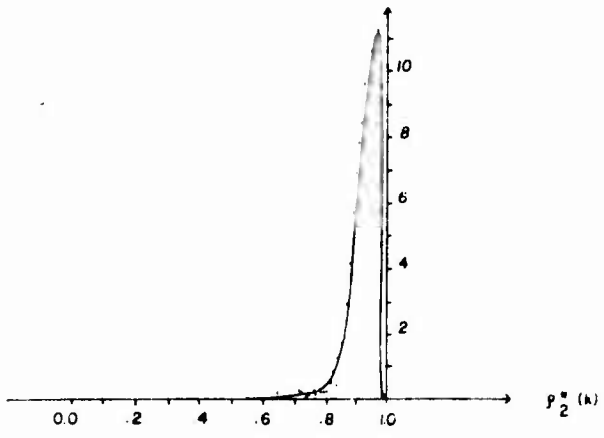

Figure 22b. Histogram of $\rho_2^*(k)$ for zero Doppler conditions. (Figure unclassified.)

histograms of $\rho_2^*(k)$, much as in the M5 and M6 experiments. Because noise can reduce the values of $\rho_2^*(k)$, making the measurement incorrect, a threshold was placed on the output signal-to-noise ratios of both $S(k, i)$ and $S(k-1, i)$. This threshold required that the signal-to-noise ratios on both $S(k, i)$ and $S(k-1, i)$ be greater than +10 db if $\rho_2^*(k)$ was to be included in the data. When this requirement is applied, approximately 100 percent of the short-range data, 56 percent of the medium-range data, and 46 percent of the long-range data meet or exceed the threshold.

(U) Figure 21a depicts the histogram of correlation coefficients $\rho_2^*(k)$ for the short-range data. The mean correlation coefficient is 0.855, with a standard deviation of 0.138. In Figs. 21b and 21c, the corresponding histograms for the medium- and long-range data are shown. The mean correlation coefficient for the medium data is 0.913, with a standard deviation of 0.112. The mean correlation for the long-range data is 0.916 with a standard deviation of 0.053. The slight increase in mean correlation value for the long-range data is not considered to be significant.

(U) The dependence of spatial stability on the relative direction of the spatial displacement is of interest. The prevailing conjecture is that the stability will be less on a full Doppler track than on a zero Doppler track. Figure 22a depicts a $\rho_2^*(k)$ histogram for the long-range data on a full Doppler track; Fig. 22b corresponds to a zero Doppler track. The mean correlation coefficient for the zero Doppler data is 0.925, with a standard deviation of 0.051; for the full Doppler track the mean and standard deviations are 0.914 and 0.053, respectively. Thus, the January 1974 data do not indicate any dependence of spatial stability on the direction of displacement, at least for long ranges.

(U) The results of the January 1974 spatial stability experiment are remarkably similar to those obtained in the M5 and M6 experiments. Figures 23a and 23b compare the overall (short medium, and long range) histogram of correlation coefficients obtained in the January 1974 experiment with a typical one-day histogram from the M6C experiment. Although the measurement interval was shorter in the January experiment than in the M6C experiment (29 sec versus 64 sec), the similarities in the histograms are amazing, considering the differences in location and range between the two experiments.

VI. FUTURE APPLICATIONS AND CONCLUSIONS

A. CONCLUSIONS

(C) The effectiveness of coherent, matched-filter techniques was demonstrated in fixed-site experiments in the Straits of Florida. The application of coherent integration over time intervals of the order of one minute yielded satisfactory operation

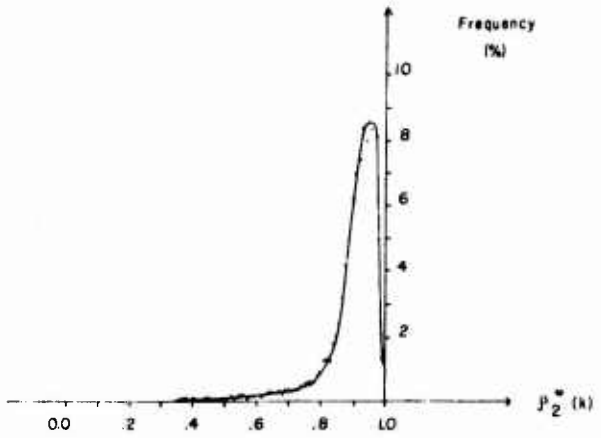

Figure 23a. Comparison of correlation coefficient histograms: overall $\rho_2^*(k)$ histogram from January 1974 experiment. (Figure unclassified.)

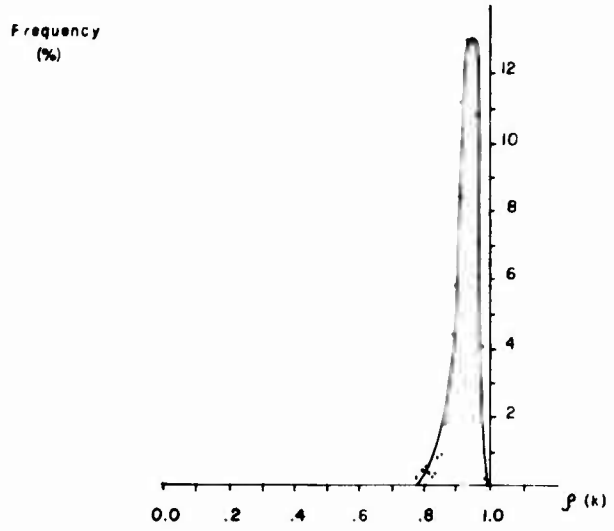

Figure 23b. Comparison of correlation coefficient histograms: one-day $\rho(k)$ histogram from M6C experiment. (Figure unclassified.)

at input signal-to-noise ratios below 0 db. By matched filtering of the received signal, the effects of selective fading and intersymbol interference due to multipath were reduced. Massive amounts of data (over 4,000 hours) on system performance add significance to the results obtained.

(C) To apply coherent, matched-filter techniques to the submarine communication problem, an understanding of the medium's spatial, as well as temporal, stability is required. A ten-day experiment in the Atlantic between Eleuthera and Bermuda with a towed source and a fixed hydrophone was conducted to measure spatial stability. The results from this experiment indicated the presence of sufficient spatial stability over intervals of at least 30 sec at six knots, at ranges from 0 to 400 nmi.

(C) The combination of fixed-site communication system results and the spatial stability measurements establishes the feasibility of coherent, matched-filter techniques for submarine communications. Advantages to be gained from these techniques include reliable operation at low signal-to-noise ratios and under varying propagation conditions. Further, randomized transmission formats can be employed to reduce the detectability of the communication signal. Because the technology required to implement coherent, matched-filter techniques is readily available, their application to submarine communications should be initiated.

1. Subsidiary Conclusions

(U) The experimental program yielded several secondary results that should be considered in subsequent submarine communication system design.

(C) First, the acoustic medium exhibits significant variance in input signal-to-noise ratio SNR_{in}, even under fixed-site conditions. Standard deviations of SNR_{in} of the order of 5 db can generally be expected. These variations require that any reliable communication system be able to operate successfully over a wide range of input signal-to-noise ratios. Coherent, matched-filter systems satisfy this requirement more closely than the incoherent systems currently in use.

(C) Second, impulsive noise must be accounted for in any system in which low (PE <0.001) bit error probabilities are required. The presence of infrequent, high-energy noise pulses can limit the error probability to a fixed level, independent of the average input signal-to-noise ratio. Soft limiting of the receiver input in conjunction with error-correcting codes can be used to overcome this limitation.

B. SUGGESTED APPLICATION

(C) The M5 and M6 communication systems were designed specifically for the evaluation of

TABLE 5. *Expected performance for the M7 system; $K_l = 4{,}000$, T 10 msec, $W = 100$ hz. (Table classified Confidential.)*

K_s	K_b	Rate, bits/sec	Minimum Operating SNR, db	Range, nmi
100	40	1.0	− 4	<100
200	20	0.5	− 7	>100
400	10	0.25	−10	>100
1000	4	0.1	−14	>100

coherent, matched-filter techniques. Consequently, their structures lack many features required of a practical submarine communication system. For example, the transmission in the M5 and M6 systems is continuous, and synchronization is performed by the operator. Neither of these characteristics is acceptable in practice. The purpose of this section is to suggest one realization of a coherent, matched-filter communications system that is suitable for operational use. Only the structure of the transmission and the expected performance characteristics are given here. The details of the receiver processing and implementation will be available in the future.

(C) Although good performance at low signal-to-noise ratios and under varying multipath conditions is necessary for any submarine communication system, other operationally important requirements must also be considered. Two such requirements are that the transmission be of limited duration and that it be detection resistant. The first requirement precludes blanking of passive sonar systems on the transmitting platform, while the second reflects the need to prevent detection or localization of the transmitting platform.

(C) The M7 system, described below, has been designed to provide an application of coherent, matched-filter techniques that satisfy the requirements previously stated. Specifically, the M7 system utilizes a burst type of transmission with a randomized format. The structure of the transmission is based entirely on an arbitrary random binary sequence that can be changed on a daily basis if desired. The only constraint on this sequence is that it must be known to both the transmitter and receiver and have the same statistical properties as other random sequences.

(C) In the M7 system, the probe and information components are phase multiplexed instead of time multiplexed as in the M5 and M6 systems. Let $u(t)$ be a low-pass digit of duration T and let f_0 be the carrier frequency, then the M7 transmission is given by

$$m(t) = \sum_{i=0}^{K_l-1} q_P(i)u(t-iT)\cos 2\pi f_0 t + q_I(i)u(t-iT)\sin 2\pi f_0 t \quad (85)$$

The first term in the sum is the probe component and the second is the information component. The coefficients $q_P(i)$, $q_I(i) \in \{\pm 1\}$ are derived from a random binary sequence $q(i)$ and the information component as indicated below.

(C) Let $q(i) \in \{\pm 1\}$ be a random binary sequence of length $2K_l$. The coefficients for the probe component $q_P(i)$ are simply the $q(i)$'s of even index:

$$q_P(i) = q(2i); \quad i = 0 \ldots K_l - 1 \quad (86)$$

Assume that K_b information bits $e(i)$ are to be transmitted. Further, assume that K_b is a factor of K_l so that $K_l = K_b \cdot K_s$ for some integer K_s. Then the coefficients for the information component are given by

$$q_I(i) = e(\lfloor i/K_s \rfloor) \cdot q(2i+1); \quad i = 0 \ldots K_l - 1 \quad (87)$$

where $\lfloor x \rfloor$ indicates the integer part of x. Thus, $q_I(i)$ is formed by the modulation of $q(i)$ for odd indices by the information values in groups of K_s digits.

(C) Since both coefficients $q_P(i)$ and $q_I(i)$ are derived from a random sequence, $q(i)$, the transmission $m(t)$ can be expected to be free from periodicities or strong spectral components. If the input signal-to-noise ratio of an intercept receiver is below 0 db, the detectability of the M7 transmission will be very low. If the input signal-to-noise ratio of the intercept receiver is above 0 db, conventional power measurement techniques are applicable. Consequently, the M7 technique (or any other) can be considered detection resistant only if the intercept receiver is denied an adequate signal-to-noise ratio, that is, be beyond a certain range.

(C) To provide an illustration of the performance to be expected of the M7 system, a specific practical example is given: Assume that the system bandwidth is 100 hz and that the transmission duration is limited to 40 sec. Let $a(t)$ be a 10-msec rectangular pulse, so that the spectrum of $a(t)$ fills the system bandwidth. Then, K_1 equals 4,000. Table 5 gives the system performance for several choices of K_2. The column marked "minimum operating SNR" gives the input signal-to-noise ratio expected to yield a bit probability of error of 0.001. This signal-to-noise ratio is obtained by taking the theoretical signal-to-noise ratio required to obtain such performance and then adding a +6 db differential to account for nonidealities. Note the low signal-to-noise ratios for which the 0.001 error probability is expected.

ACKNOWLEDGMENTS

(U) This project was supported by the Defense Advanced Research Projects Agency and the Office of Naval Research through Dr. Alan O. Sykes, ONR Code 412. Portions of the effort were performed at the Rosenstiel School of Marine and Atmospheric Sciences, University of Miami (N00014-67-A-0201-0020) and at the Institute for Acoustical Research, Palisades Geophysical Institute (N00014-73-C-0434).

(U) The assistance of Cmdr. D. Kuehler and company of the U.S. Naval Facility, Eleuthera during the January 1974 experiments is gratefully acknowledged.

(U) Special appreciation is due to Dr. Chester A. Jacewitz, Mr. John J. Shearer, and Ms. Mary Forlenza for their contributions to the research program.

REFERENCES

1. C. V. Kimball, "Intersymbol Interference in Binary Communication Systems," Tech. Rpt. 195, Cooley Electronics Laboratory, University of Michigan, Ann Arbor, Mich., August 1968.
2. C. V. Kimball, "A MIMI Communication Experiment," Tech. Rpt. 197, Cooley Electronics Laboratory, University of Michigan, Ann Arbor, Mich., June 1973 (Confidential-NF).
3. D. Jaarsma, "Experimental Research in Binary Communications Using the Miami 42-Mile Underwater Acoustic Channel," Tech. Rpt. 207, Cooley Electronics Laboratory, University of Michigan, Ann Arbor, Mich., 1974 (Confidential-NF).
4. J. C. Steinberg and T. G. Birdsall, "Underwater Sound Propagation in the Straits of Florida," *J. Acoust. Soc. Am. 39*, 301 (1966).

(U) DISTRIBUTION LIST

	COPY NO.
Advanced Research Projects Agency 1400 Wilson Blvd. Arlington, Virginia 22209	
Attn: Dr. R. Seesholtz	1
Dr. R. Cook	2
Office of Naval Research (Code 222) 800 N. Quincy St. Arlington, Virginia 22217	
Attn: Dr. A. O. Sykes	3-5
Director Naval Research Laboratory Washington, D. C. 20390	
Attn: Dr. William Hahn	6
Mr. Caldwell McCoy	7
Technical Information Division	8-12
Commander Naval Ordnance Laboratory Acoustics Division White Oak, Silver Spring, Maryland 20907	
Attn: Dr. Zaka Slawsky	13
Commander Naval Undersea Center San Diego, California 92132	
Attn: Mr. Darrell Marsh	14
Dr. Harper Whitehouse	15
Commanding Officer & Director Naval Underwater Systems Center Fort Trumbull New London, Connecticut 06321	
Attn: Dr. A. Ellinthorpe	16
Dr. A. Nuttal	17
Dr. D. Viccione	18
Commander Naval Air Development Center Johnsville, Warminster, Pennsylvania 18974	19
Commanding Officer Naval Ship Research & Development Center Washington, D.C. 20034	20

(U) DISTRIBUTION LIST (Cont.)

	COPY NO.
NISC 4301 Suitland Road Washington, D. C. 20390 Attn: Johann Martinek Mr. E. Bisset	 21 22
Commander Naval Ordnance Systems Command Code ORD-03C Navy Department Washington, D. C. 20360	 23
Commander Naval Sea Systems Command Code Washington, D. C. 20360 Attn: Mr. Carey D. Smith Mrs. Dolly Hoffman	 24 25
Commander Naval Undersea Research & Development Center 3202 E. Foothill Blvd. Pasadena, California 91107	 26
Naval Electronics Systems Command Washington, D. C. 20360 Attn: Mr. M. Parker Mr. I. Smietan	 27 28
Naval Electronics Systems Command Submarine Integration Division PME 117-23 Washington, D. C. 20360 Attn: Mr. Weinberger	 29
Chief of Naval Operations 801 N. Randolph Street Arlington, Virginia 22203 Attn: Code OP-095C	 30
Defense Documentation Center Cameron Station Alexandria, Virginia 22314	 31-32
Dr. Harry Sonnemann Office of the Assistant Secretary of the Navy (Research & Development) Room 4D745, Pentagon Washington, D. C. 20350	33
Dr. James Probus Director of Naval Laboratory Room 1062, Crystal Plaza Bldg. 5 Dept. of Navy Washington, D. C. 20390	34

(U) DISTRIBUTION LIST (Cont.)

	COPY NO.
Dr. T. G. Birdsall Cooley Electronics Laboratory University of Michigan Ann Arbor, Michigan 48105	35
Dr. Hollis Boehme Applied Research Lab University of Texas Austin, Texas	36
Dr. John Bouyoucos Hydroacoustics, Inc. P. O. Box 3818 Rochester, New York 14610	37
Dr. Scott C. Daubin Ocean Engineering Dept. RSMAS 4600 Rickenbacker Causeway Miami, Florida 33149	38
Dr. David Jaarsma Planning Systems, Inc. McLean, Virginia 22101	39
Dr. C. V. Kimball Ocean Engineering Dept. RSMAS 4600 Rickenbacker Causeway Miami, Florida 33149	40-49
Dr. Thomas G. Kincaid General Electric Company P. O. Box 1088 Schenectady, New York	50
Mr. Charles Loda Institute for Defense Analyses 400 Army-Navy Drive Arlington, Virginia 22202	51
Dr. Loren W. Nolte c/o U.S. Army Research Office - Durham Box CM - Duke Station Durham, North Carolina	52
Dr. John Pierce Signatron Corporation Boston, Massachusetts	53
Dr. Robert Price Sperry Research Center Sudbury, Massachusetts	54

(U) DISTRIBUTION LIST (Cont.)

	COPY NO.
Dr. L. Scharf Electrical Engineering Department University of Colorado Ft. Collins, Colorado	55
Dr. Ed Titlebaum College of Engr./Applied Science University of Rochester River Station Rochester, N. Y. 14627	56
Dr. Julio Torres Riverside Research Institute 1701 N. Ft. Meyer Drive Suite 711 Arlington, Virginia 22209	57
Dr. Ray Veenkant Texas Instruments, Inc. 13500 North Central Expressway Dallas, Texas 75231	58
Dr. B. Widrow Stanford Electronics Laboratory Stanford, California 94305	59
Mr. M. Kronengold Palisades Geophysical Institute 615 SW 2nd Ave. Miami, Florida	60

UNCLASSIFIED

SECURITY CLASSIFICATION OF THIS PAGE (When Data Entered)

CONFIDENTIAL

REPORT DOCUMENTATION PAGE		READ INSTRUCTIONS BEFORE COMPLETING FORM
1. REPORT NUMBER UM-RSMAS 75034	2. GOVT ACCESSION NO.	3. RECIPIENT'S CATALOG NUMBER
4. TITLE (and Subtitle) Acoustic Communication Studies (U)		5. TYPE OF REPORT & PERIOD COVERED Technical Report July 1971 - June 1974 6. PERFORMING ORG. REPORT NUMBER
7. AUTHOR(s) Kimball, Christopher V.		8. CONTRACT OR GRANT NUMBER(s) N00014-73-C-0593
9. PERFORMING ORGANIZATION NAME AND ADDRESS Ocean Engineering Division, RSMAS University of Miami 4600 Rickenbacker Csw. Miami, FL 33149		10. PROGRAM ELEMENT, PROJECT, TASK AREA & WORK UNIT NUMBERS
11. CONTROLLING OFFICE NAME AND ADDRESS Office of Naval Research (Code 222) 800 N. Quincy St. Arlington, Virginia		12. REPORT DATE September 1975 13. NUMBER OF PAGES
14. MONITORING AGENCY NAME & ADDRESS(if different from Controlling Office) As in 11 above.		15. SECURITY CLASS. (of this report) CONFIDENTIAL 15a. DECLASSIFICATION/DOWNGRADING SCHEDULE Ex Cat 3 Declass 31 Dec 2005

16. DISTRIBUTION STATEMENT (of this Report)

Distribution limited to U.S. Government Agencies only; Test and evaluation. 1 July 1975 Other requests for this document should be referred to the Office of Naval Research (Code 222).

17. DISTRIBUTION STATEMENT (of the abstract entered in Block 20, if different from Report)

As in 16 above.

18. SUPPLEMENTARY NOTES

To be published in the Journal of Defense Research, Series B: Tactical Warfare, September 1975.

19. KEY WORDS (Continue on reverse side if necessary and identify by block number)

Underwater Acoustics
Communication Systems

20. ABSTRACT (Continue on reverse side if necessary and identify by block number)

(u) An experimental study of techniques for submarine to submarine communication was conducted. Based on the results of the experimental program, a practical submarine to submarine communication system is proposed. A particular implementation (M7) is suggested as a basis for future work.

CONFIDENTIAL

DD FORM 1 JAN 73 1473 EDITION OF 1 NOV 65 IS OBSOLETE
S/N 0102-014-6601 |

UNCLASSIFIED
SECURITY CLASSIFICATION OF THIS PAGE (When Data Entered)

CONFIDENTIAL

CONFIDENTIAL

DEPARTMENT OF THE NAVY
OFFICE OF NAVAL RESEARCH
875 NORTH RANDOLPH STREET
SUITE 1425
ARLINGTON VA 22203-1995

IN REPLY REFER TO
5513
Ser 43/020
18 Jul 16

From: Chief of Naval Research
To: Chief of Naval Operations DNS-36

Subj: MANDATORY DECLASSIFICATION REVIEW ON FREEDOM OF INFORMATION ACT REQUEST ONR 16-061

Ref: (a) SECNAVINST M-5510.36
(b) Chief of Naval Operations DNS-36 ltr dtd 15 Apr 2016; ref: 11F-0407/13F-1279

Encl: (1) Acoustics Communications Studies (U)

1. In accordance with reference (a), a declassification review per reference (b), has been conducted on enclosure (1). A determination has been made that the material contained in enclosure (1) under Office of Naval Research (ONR) original classification authority is hereby declassified and shall be treated and handled as unclassified.

2. You may contact Mr. Derrick Shack (ONR 43) at 703-696-1499 or by email at derrick.shack@navy.mil for any questions regarding this matter.

MATHIAS W. WINTER
Rear Admiral, U.S. Navy

Copy to:
DTIC
CNO DNS-36
ONR FOIA